Journal of Solid State Electrochemistry (2019) 23:1061–1081
https://doi.org/10.1007/s10008-019-04211-x

REVIEW

Advanced carbon electrode for electrochemical capacitors

Yuya Kado[1] · Yasushi Soneda[1] · Hiroaki Hatori[1] · Masaya Kodama[1]

Received: 17 October 2018 / Revised: 29 January 2019 / Accepted: 3 February 2019 / Published online: 11 February 2019

Abstract

Electrochemical capacitors are high-power energy storage devices having long cycle durability in comparison to secondary batteries. The energy storage mechanisms can be electric double-layer capacitance (ion adsorption) or pseudocapacitance (fast redox reaction) at the electrode-electrolyte interface. Most commonly used electrode materials are carbon materials with high specific surface area, microporous-activated carbons. A considerable number of studies have been conducted to optimize the pore structure and surface functionalities of activated carbons. In addition to conventional activated carbons, other types of carbon materials such as carbon aerogel/xerogel, templated carbons, carbide-derived carbons, carbon nanotubes, and graphene-based materials have been investigated. This review highlights the key features of advanced carbon materials for application to commercial capacitor devices.

Keywords Electrochemical capacitors · Electrode materials · Advanced carbons · Pseudocapacitances

Introduction

Since the Paris Agreement, global energy requirements have accelerated toward the need for clean energy, which has prompted further electrification of energy for the world economy [1]. Electrification of energy comprises the stages of generation, transmission, distribution, and utilization. Electric energy storage is a key technology to support the above processes, as it can help to meet the flexible supply and demand of electrical energy. Because of their high power densities and long life cycles, electrochemical capacitors have attracted significant interest for several applications, such as portable energy devices, power-assist systems in electric (hybrid) vehicles, and for load leveling of renewable energy generation (e.g., solar, wind) [2–5]. The most typical and fundamental electrochemical capacitor device is the electric double-layer capacitor (EDLC), which stores energy in an electrostatic manner—accumulation of negative and positive charges on the surface of electrodes (non-Faradaic process) in a symmetrical configuration—as illustrated in Fig. 1. Carbon materials are usually used as electrode materials because of their unique properties, such as high electrical conductivity, chemical stability in different solutions (acidic, basic, organic), easy processability, controllable porosity, and low cost [6, 7]. Indeed, several types of carbon materials (activated carbons, carbon aerogels, templated carbons, carbon nanotubes, etc.) have already been studied for electrochemical capacitor as summarized in Fig. 2 and Table 1.

Among them, microporous-activated carbons with high specific surface area are the most commonly used electrode materials for EDLCs. In principle, owing to the energy storage mechanism, a high specific surface area is important for storing a large amount of energy. However, the performance of EDLCs significantly depends not only on the surface area but also on the pore size distribution of carbon materials. Consequently, numerous efforts have been made to optimize the pore structure of carbon materials [6–8, 25–27]. Micropores (< 2 nm in diameter), which are accessible to electrolytes play an important role in capacitive behaviors in aqueous and non-aqueous solutions [9, 28]. In addition, using carbide-derived carbons, Chmiola et al. demonstrated that anomalous increases in capacitance occur for at pore sizes of less than 1 nm, and Largeot et al. reported that a pore size equal to the ion size is the most effective size for high capacitance in ionic liquids [16, 29]. Thus, although the micropore contribution to EDLC performance is clearly significant, the mesopores (2–50 nm in diameter) are considered more favorable for high-power applications, because ions can migrate more readily through mesopores than

✉ Yasushi Soneda
y.soneda@aist.go.jp

[1] Energy Conversion Materials Group, Research Institute of Energy Frontier, National Institute of Advanced Industrial Science and Technology (AIST), 16-1 Onogawa, Tsukuba, Ibaraki 305-8569, Japan

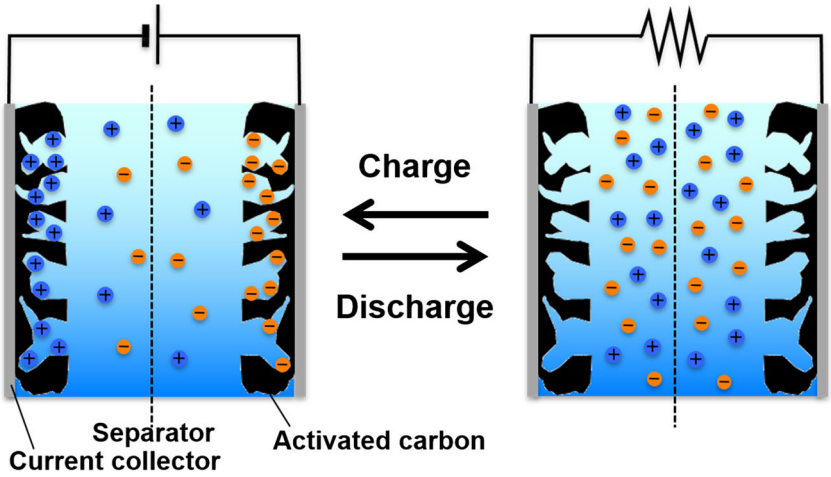

Fig. 1 Schematic drawing of EDLC operation

through micropores [8, 27]. Therefore, it is essential to control the pore size distribution (the ratio of micropores to meso/macropores) to achieve enhanced capacitive performance. This condition is also important to realize large energy and power density per unit volume in EDLCs, because the volumetric characteristics are strongly influenced by the density of the electrode materials [3, 7, 30, 31]. However, it is difficult to control the pore size distribution of activated carbons produced by the activation process using an oxidation reaction with water vapor and/or other chemicals. In this view, the template method is one of the most effective techniques to obtain the controlled pore structures of carbons, in which a hard template (that must be removed with a post treatment) or a soft template (that decomposes during the synthesis process) is used [32, 33]. The most attractive point of the template method is that the pore size distribution of the mother template is transferred to the carbon materials, which enables a relatively narrow pore size distribution. Various templated carbons have been synthesized to control their morphology and pore structure for use as electrode materials in EDLCs [33–35]. Among them, MgO-templated carbons are now produced on a mass scale, and they currently are the most feasible templated carbons for industry [36]. Another promising strategy to control the pore structure of carbons is a sol-gel route using organic aerogels, mostly based on resorcinol and formaldehyde; the obtained carbon aerogels possess a large amount of mesopores with interconnected carbon networks [6, 7, 14, 15]. In this method, the gel preparation conditions, such as the basic catalyst concentration and pH of the solution, determine the pore structure of the final-product carbons.

Other carbon nanomaterials, such as carbon nanotubes [37–42] and more recently graphene-based materials [23, 43–48] have attracted attention as innovative capacitor electrode materials. An EDLC electrode, in principle, must be electrically conductive and remain inert during charge/discharge process. However, activated carbons possess insufficient electrical conductivity and must be used with conductive additives such as carbon black, [3] which reduces the effective carbon mass loading in a carbon electrode. Moreover, activated carbons are composed of small structural units of turbostratic carbon having multiple electrochemical active sites (graphene edges with functional groups). On the other hand, a graphene, ideally, has high electrical conductivity (high electron mobility), and the basal plane of graphene is

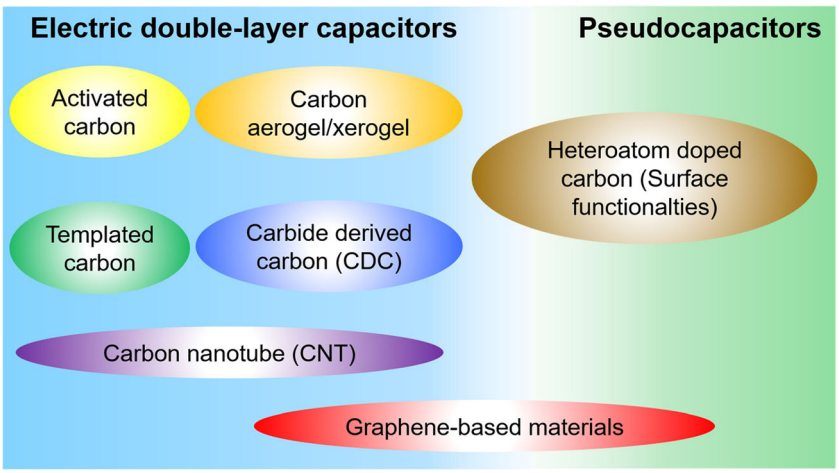

Fig. 2 Carbon materials used as primary electrode materials for electrochemical capacitors

Table 1 Reported surface area and capacitance value of various carbon materials (2-E, 3-E: two- or three-electrode system)

Material and method	Surface area/m^2 g^{-1}	Electrolyte	Capacitance/F g^{-1} (Cell configuration)	Ref.
Activated carbon				
Coal/steam AC	1270	1 M H_2SO_4	147 (2-E)	[8]
		6 M KOH	124 (2-E)	[8]
Coal/KOH AC	3030	6 M KOH	260 (2-E)	[9]
Coconut shell/steam AC	1550	1 M $TEMABF_4$/PC	25 (2-E)	[10]
Templated carbon				
Furfuryl alcohol/silica	1880	1 M H_2SO_4	199 (2-E)	[11]
		6 M KOH	205 (2-E)	[11]
		1 M $TEABF_4$/AN	113 (2-E)	[11]
C_2H_2/Zeolite	3040	1 M $TEABF_4$/PC	168 (3-E)	[12]
Mg citrate/MgO	2100	40% H_2SO_4	470 (3-E)	[13]
		1 M $TEABF_4$/PC	30 (2-E)	[13]
Carbon aerogel/xerogel				
Resorcinol-Formaldehyde	1340	0.8 M $TEABF_4$/PC	108 (2-E)	[14]
Resorcinol-Formaldehyde	800	30% H_2SO_4	185 (3-E)	[15]
Carbide-derived carbon				
TiC	1270	1.5 M $TEABF_4$/AN	143 (2-E)	[16]
Carbon nanotube				
SG-SW sheet	530	1 M $TEABF_4$/PC	20 (2-E)	[17]
HiPco-SW sheet	726	1 M $TEABF_4$/PC	70 (3-E)	[18]
HiPco-DW sheet	588	1 M $TEABF_4$/PC	45 (3-E)	[18]
Heteroatom-doped carbon				
O (Na alginate)	270	1 M H_2SO_4	19 (2-E)	[19]
N (Pyridine/mica template)	83	1 M H_2SO_4	182 (3-E)	[20]
N (Melamine foam)	< 1	1 M H_2SO_4	240 (3-E)	[21]
B (Sucrose-Boric acid)	660	1 M H_2SO_4	110 (3-E)	[22]
Graphene-based materials				
rGO	705	5.5 M KOH	135 (2-E)	[23]
		1 M $TEABF_4$/PC	95 (2-E)	[23]
ExCF (Mesophase pitch)	300	18 M H2SO4	450 (3-E)	[24]

less active in redox reactions than its edge plane. Although monolayer graphene has a theoretical surface area of 2630 m^2 g^{-1}, multilayered graphene composed of stacked graphene layers produces a lower effective surface area. To provide high-surface-area graphene electrodes, various types of pore structure control techniques such as oxidative activation, template methods, and fabrication of foam or aerogel morphologies have been performed [45–47]. Combination with nanosized particles, fibers and tubes to avoid agglomerations that cause layer stacking, thus providing effective surface area and pore channels for the adsorption and transportation of ions, is a characteristic strategy for preparing the graphene-based materials [45, 48]. A carbon nanotube (CNT), especially a single-walled carbon nanotube (SWCNT) which has a hollow fibrous form obtained by seamlessly rolling a graphene, has a basal plane with a large surface area without active edge sites provided it has integrity and a high aspect ratio. CNT, a molecular-like building block, is one of the ideal EDLC electrode materials with high electrical conductivity and inactivity, and its 3D features provide useful design capability for forming a high-surface-area electrode. From the application viewpoint, highly conductive materials allow for electrodes with high power density and durability and an inactive surface for redox reactions, leading to a high working cell voltage that contributes to both the energy and power densities of capacitor devices using organic electrolytes. Recent progress in the mass production of pure SWCNT has enabled investigation of electrode performance from both application and commercialization viewpoints, as well as the actual fabrication of a 1000 F class capacitor cell suitable for power regeneration [49]. Because the intrinsic nature of solid electrode materials and pore structure design remarkably influence the EDLC device performance, we focused on this area as the second topic in this review.

In addition to nanostructure engineering, the chemistry of surface functionalities and heteroatom doping in the carbon framework have been explored to improve capacitive performance. These techniques often involve Faradaic reactions to develop pseudocapacitors. Because the most obvious shortcoming of EDLCs is their smaller energy density than that of secondary batteries such as lithium ion batteries (LIBs), introducing pseudocapacitance is one of the approaches that can be used to increase the energy density of capacitors [50–52]. A considerable number of studies have been conducted on pseudocapacitors or hybrid (asymmetric) capacitors. Surface functional groups of carbon materials [19, 21, 53–59], conducting polymers [60–62], transition metal oxides [63–66], and their composite electrodes [67, 68] with carbon additives as a conducting support have also been investigated. Among these materials, conducting polymers and transition metal oxides can provide relatively high capacitance, but carbon materials are most advantageous in view of low cost, easy processability, and eco-friendliness. In addition, as these pseudocapacitive behaviors significantly depend on both the electrolyte and electrode materials, matching electrode materials with electrolytes is also one of the key technologies to enhance capacitor performance.

Thus, carbon materials are at the center of discussion as promising electrode materials for electrochemical capacitors involving Faradaic or non-Faradaic reactions to store energy in symmetric or asymmetric configurations. In this review, we highlight the key features of carbon materials as primary electrode materials for commercial capacitor devices in the future.

Templated carbon

EDLC performance of templated carbons

Various template materials, such as anodized alumina [69, 70], mesoporous silica [11, 34, 71–73], zeolites [12, 35, 74], colloidal silica [75], and magnesia [33, 36, 76–79] have been used for synthesis of templated carbons. The preparation of templated carbons generally involves the incorporation of a carbon precursor (such as sucrose, furfuryl alcohol, acetylene, or phenol resin) through either a solution-phase or a vapor-phase reaction into a hard template, followed by the pyrolysis of the carbon precursor. The elimination of the template materials often requires the use of hydrofluoric acid or high-concentration alkali solutions in a hard-template method. For example, Fig. 3 shows a synthesis process of zeolite-templated carbon (ZTC) with three-dimensionally connected micropores reported by Nishihara et al. [74]. Carbon is loaded into the nanochannels of the zeolite framework and then ZTC with micropores of ca. 1.2 nm in diameter is obtained after the zeolite is washed by a hydrofluoric acid solution. Using ZTCs as electrode materials for EDLCs, Nishihara et al. reported that such a three-dimensionally ordered micropores significantly enhanced the ion transfer compared with microporous-activated carbons having very broad pore size distributions [12].

MgO-templated carbons are typical mesopore-dominant materials with high specific surface areas and can be produced more easily because dilute acids are applicable to dissolve the MgO templates unlike silica or zeolite templates [13, 80–83]. Indeed, MgO-templated carbons are now produced on an industrial scale and are available to buy on the market under the product name CNovel. The details of the production method are described in the literature [33, 36]. Kado et al. reported the correlation between the pore structure and electrode density of the MgO-templated carbon electrodes for EDLCs in organic electrolyte as summarized in Fig. 4 [82]. The obtained MgO-templated porous carbons (MPCs) are denoted as MPC-1, MPC-10, MPC-20, and MPC-40, where the numbers correspond to the different ramping rates used (°C min^{-1}). N_2 isotherm shown in Fig. 4a presented that the faster heating rates resulted in larger mesopores being produced and greater mesopore volumes. As a result, it is possible to control the pore size distribution of the MgO-templated carbons derived from magnesium citrate only by changing the heating rate in the carbonization process. Thus, the MPCs have the advantage of a high specific surface area (~2000 m^2 g^{-1}) originating from the presence of both micropores and mesopores. However, the electrode density decreased upon an increase in the pore volume, particularly mesopore volume, of carbons as shown in Fig. 4b, which is closely linked to capacitance per volume [84, 85]. Indeed, the volumetric capacitance of MPCs was lower than that of microporous-activated carbon (YP-17) at a current density of 0.1 A g^{-1} due to their small electrode densities, except MPC-1 with the largest electrode density of 0.48 g cm^{-3} (Fig. 4c). However, at 10 A g^{-1}, the MPCs with a large mesopore volume were clearly observed to have greater volumetric capacitance values than that of YP-17. This result indicates that the positive effect of the presence of mesopores on the rate capability is more significant than the negative effect of the small electrode density. It should be noted that the positive effect is limited, when comparing MPC-10 with MPC-20 or MPC-40 **(**Fig. 4**c).** This indicates that the rate performance is significantly enhanced by the presence of a small number of mesopores, but the effect of further increasing the number of mesopores is relatively small. Thus, the observed rate capabilities of the MPCs were remarkable, which was attributed to the presence of mesopores as an accessible ion pathway [8, 27]. On the other hand, there has been some reports claiming that the better performance at a high rate is ascribed to a lower content of oxygen functionalities (in particular, CO_2-desorbing groups) of templated mesoporous carbons rather than to their pore structures [86, 87]. But, no clear influence of the carboxylic groups on the rate capability was observed in the case of MgO-templated

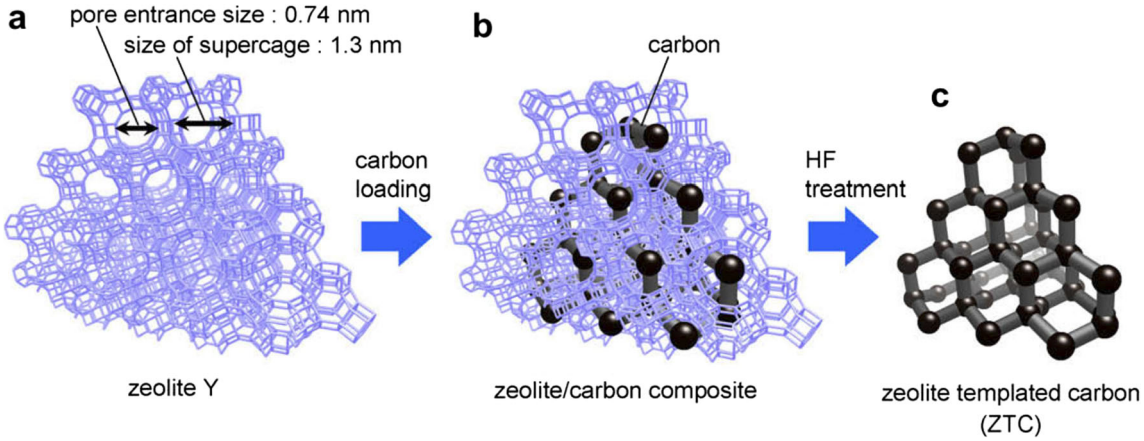

Fig. 3 Synthesis process of the zeolite-templated carbon (ZTC). Reprinted with permission from ref. [74]. Copyright 2008 Elsevier

carbons. These outstanding effects of mesopores on the ion diffusion were also observed in low-temperature operations; mesopores of carbon materials can provide a smooth pathway for the ions, minimizing the elevation of the diffusion resistance at low temperatures [13, 80]. To further investigate the relationship between the pore volume and electrode density, the theoretical maximum value for the electrode density was calculated as shown in Fig. 4d (the details are described in the literature [82]). In a similar manner to that of the calculated values, the measured electrode densities decreased upon an increase in the pore volumes of the carbons. The differences between the measured and calculated values can be attributed to the void spaces between the carbon particles. The maximum ratio of the measured and calculated densities was only

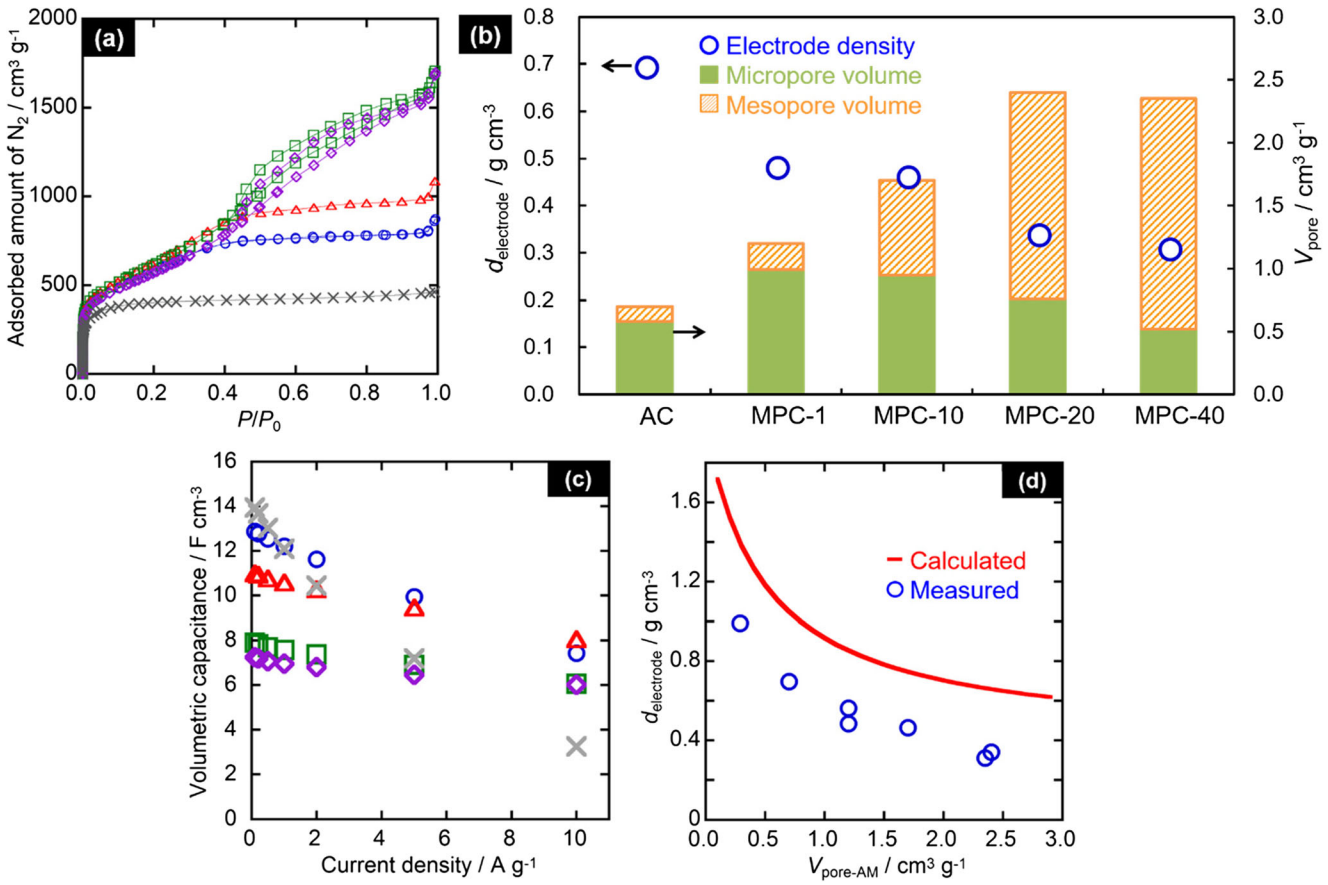

Fig. 4 **a** N_2 isotherms of carbons. **b** Relationship between electrode density, mesopore volume, and micropore volume. **c** Volumetric capacitance at each current density. **d** Relationship between the electrode density and total pore volume (solid line: theoretical maximum density, circle: measured density). The symbols in (**a**, **c**): white circle, white triangle, white square, diamond, multiplication sign, denote MPC-1, MPC-10, MPC-20, MPC-40, and YP-17 for comparison. Reproduced with permission from ref. [82]. Copyright 2016 Elsevier

70%, indicating that the electrode density could be further improved by reducing the number of void spaces between the carbon particles, although a certain amount of space is required for electrolyte penetration.

Thus, the pore structures of carbons can be tuned effectively by template methods and the EDLC performances of templated microporous and mesoporous carbons have been studied. In recent years, efforts have been made to elucidate the degradation mechanism and improve the charging voltage of EDLCs using carbon materials [10, 17, 83, 88–92]. According to the literature, capacitance loss is mainly caused by the electrochemical decomposition of electrolytes at the electrode surfaces and/or in the pores. One of the causes of electrochemical decomposition is the presence of oxygen functionalities on the carbons, which work as electrochemically active sites. For instance, Shiraishi reported that reducing the number of oxygen functionalities of the activated carbons by heat treatment resulted in better durability [90]. Another major issue is the breakdown of the electrical network in the carbon electrode caused by the decomposition products or generated gases. According to Shiraishi's work, a boundary-free electrode structure, as well as a porous current collector, is effective in improving the durability of the system, because of the robust electrical networks in the electrode [10]. The addition of carbon nanotubes to the electrode was also found to enhance the durability by maintaining the electron conductivity in the electrode (discussed in the last part of "Electrode design based on the formability of CNTs" section) [17]. Most of these investigations involved the use of microporous-activated carbons. Recently, Kado et al. reported the durability and degradation behaviors of MgO-templated mesoporous carbons, CNovel, in comparison with those of microporous activated carbons [83]. Table 2 shows the results of durability tests using these carbons were conducted under floating conditions: 3.0 or 3.2 V/70 °C/100 h. A comparison of the capacitance retention values at low current densities (0.1 or 1.0 A g^{-1}) revealed that YP50F is slightly more durable than CNovel. However, at high current densities (4.0 A g^{-1}), the capacitance retention of CNovel was much higher than that of YP50F. This remarkable durability at high current densities can be explained by the fact that CNovel showed a relatively lower increase in equivalent series resistance (ESR) than YP50F after the durability test. On the other hand, CNovel showed a much greater leak current density than YP50F. The origin of the leak current density is a Faradaic reaction, indicating that the electrolyte decomposition was more significant for CNovel than for YP50F. One possible reason is that mesopore surfaces are more electroactive than micropore surfaces. When mesoporous carbons are employed as anode materials in lithium- or sodium-ion batteries, a huge irreversible capacity is observed due to the formation of a solid electrolyte interface (SEI) layer caused by the electrochemical decomposition of the electrolyte [93–96]. It is proposed that solvated ions can pass more readily through mesopores than through micropores to the active surface area of the carbons for decomposition. It is deduced that the degradation mechanism of EDLCs made using templated mesoporous carbons is different from that of EDLCs made using microporous carbons. Note that no clear influence of the oxygen functionalities was confirmed in case of the MgO-templated mesoporous carbon [83].

Figure 5a, b shows the pore size distributions of the carbon electrodes before and after the durability test, that was estimated using quenched solid density functional theory (QSDFT). In the case of YP50F, the volume of the micropores decreased, but the size of the micropores was unchanged, suggesting that the decomposition products did not accumulate inside the micropores but instead deposited around the entrance of the micropores. On the other hand, for CNovel, the peak mesopore size decreased as the mesopore volume decreased, indicating that the decomposition products accumulated inside the mesopores. This trend possibly affects the diffusion of ions, because the presence of mesopores is vital for the high-rate performance of CNovel. However, AC impedance measurements showed that the charge transfer resistances significantly increased rather than the distributed resistances for both YP50F and CNovel. This could be attributed to deposition of the solid products around the entrance of the micropores. Notably, CNovel maintained a low ion diffusion resistance despite the decomposition products being deposited inside the mesopores because of a sufficiently large number of mesopores for fast ion migration even after the durability test, leading to its remarkable durability at high current densities. Thus, it can be concluded that although the mesopores unfortunately promote electrolyte decomposition, their influence on the capacitive performance is not significant because the decomposition products are deposited in the mesopores without increasing the diffusion resistance of the ions. Nonetheless, the high leak current is one of the challenging problems in practical operations of capacitor devices. It is still controversial which electrode dominates the capacitance loss, positive or negative electrode in PC-based solution [83, 89, 91, 92, 97]. The degradation behavior must be made clearer in the future work for further improvement of EDLCs using carbon materials.

Application of templated carbons to anode materials for Na ion energy storage

The amounts of energy that can be stored in EDLCs is heavily limited by the energy storage mechanism as discussed above. In recent years, lithium (Li) insertion to bring about pseudocapacitance in electrode materials such as TiO_2 [98], MnO_3 [99], Fe_2O_3 [100, 101], and carbon [93, 102] has been explored because Li-based capacitors or batteries are very promising energy storage systems due to their high-energy densities [103–106]. However, given the increasing demand

Table 2 Results of the durability test at 3.0 and 3.2 V. Reproduced with permission from ref. [83]. Copyright 2017 Carbon Society of Japan

Rot No.	Voltage/ V	Capacitance retention[a]/%			ESR ratio[b]	LC[c]/ mA g^{-1}
		0.1 A g^{-1}	1 A g^{-1}	4 A g^{-1}		
YP50F-1	3.0	92	80	53	1.5	1.9
YP50F-2	3.2	87	70	33	2.0	2.7
CNovel-1	3.0	88	80	73	1.4	9.3
CNovel-2	3.2	76	66	54	1.7	18

[a] Retention at each current density after the durability test

[b] Ratio of the equivalent series resistance before and after the durability test which was estimated by the IR drop in the discharge curves

[c] Leak current density determined as the current density after 100 h during the durability test

for Li-based systems, there is concern about the depletion of Li resources, which are limited and unevenly distributed in the world. Thus, sodium (Na) has attracted interest as an alternative to Li for use in energy storage systems in view of its low cost and abundance (the Clarke of Na is 500 times greater than that of Li) [107–109]. Recently, carbon materials such as nonporous hard carbon and mesoporous carbon prepared using different methods have been studied for use in Na-ion batteries or capacitors [94–96, 110–122]. By templating strategies, Wenzel et al. have demonstrated the improved rate capability of silica-templated carbons [113]. Tang et al. also have reported hollow carbon nanospheres with superior rate capability that was made by soft templating method as shown in Fig. 6a, b [114]. Uniformly shaped hollow nanospheres having a specific surface of 410 m^2 g^{-1} was produced, and a capacity of 50 mAh g^{-1} was maintained even at 10 A g^{-1} due to such a unique structure. The reaction scheme is illustrated in Fig. 6c claiming that, in addition to the efficient electron transfer through the well-connected hollow carbons, a large specific surface area offered a large number of active sites for charge transfer reactions and the large interlayer spacing facilitated the transport and storage of Na between the graphene layers.

Very recently, Kado et al. investigated the Na ion storage of MgO-templated mesoporous carbons (CNovel) in comparison to a commercial hard carbon (LN-0001) for application to Na ion capacitors as summarized in Fig. 7 [94–96]. Cyclic voltammograms showed the reduction/oxidation peaks at approximately 0.1 V vs. Na^+/Na in both materials (Fig. 7a), which are attributed to Na insertion into the carbon layers. The peaks were observed to be much sharper for the hard carbon electrode than for CNovel. This increase in sharpness is due to the difference in the crystallinity of each carbon. CNovel was annealed at a relatively low temperature (1000 °C); therefore, its carbon layers contain fewer Na-insertion sites compared to the carbon layers of the hard carbon. In addition, capacitive contributions were observed to be significant for CNovel due to its large specific surface area, and no plateau region was observed in the potential profiles in charge-discharge tests (Fig. 7b). The CNovel electrode exhibited a discharge (Na-deinsertion) capacity of 180 mAh g^{-1}, which is comparable to that of the hard carbon electrode at low current density. The most remarkable result was the excellent rate capability, as shown in Fig. 7c, which is in good agreement with the above studies [113, 114]. It was concluded that Na-ion storage mechanism in the MgO-templated mesoporous carbons is the combination of Faradaic Na intercalation in the carbon layers and non-Faradaic electric double-layer capacitance. In this view, the appropriate balance between crystallinity and pore structure of carbon is important for Na-ion storage. The challenging problem of porous carbons for Na ion storage is the huge irreversible capacity and very low coulombic efficiency of the first cycle. This is attributed to the formation of SEI layers on the carbon electrode surfaces and is significant for high-surface area carbons [93, 96]. The coulombic efficiency was less than 30% for these templated carbons, and this low value is an issue that must be solved for Na-ion battery applications. However, the use of these templated carbons as negative electrode materials for Na-ion capacitors is promising because the irreversible behavior is not observed after pre-doping which is an essential pretreatment for operation of hybrid capacitor systems. Figure 7d shows the relationship between the energy density and power density (the Ragone plots) using YP-17 and CNovel as the positive and negative electrode materials (denoted as the YP-CN cell). For comparison, another full cell was assembled using YP-17 and LN-0001 as the positive and negative electrodes (denoted as the YP-LN cell). Pre-doping of CNovel and LN-0001 was performed by short-circuiting for 24 h using Na foils as the counter electrodes. Their energy densities were comparable at a low power density, but the YP-CN cell exhibited a significantly greater energy density than the YP-LN cell at a high power density. This was attributed to faster Na-ion storage in the CNovel negative electrodes. In addition, it should be noted that cycle-life measurements showed 90% retention and coulombic efficiencies of almost 100% after 1000 cycles for both cells. These results further confirm that MgO-templated carbon shows promise for use as a negative electrode material in Na-ion capacitors.

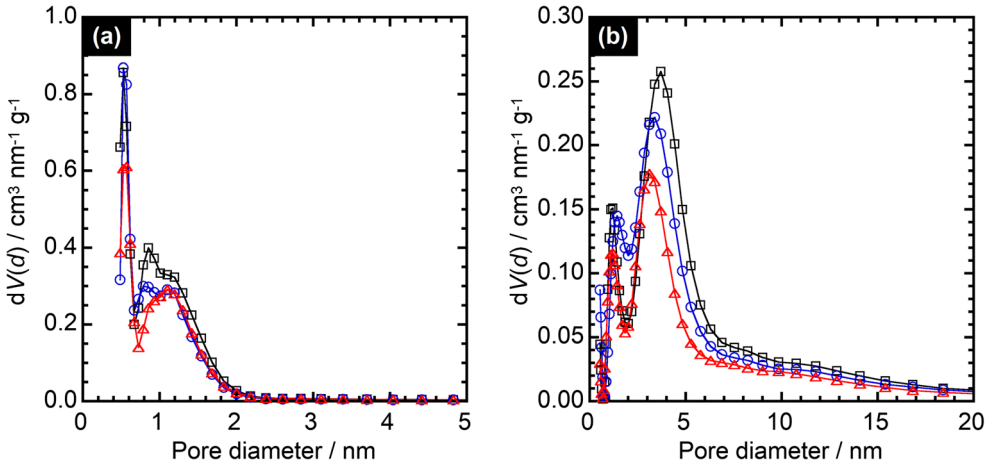

Fig. 5 QSDFT pore size distributions of **a** YP50F and **b** CNovel electrodes before and after the durability test (white square: fresh electrode, white circle: aged positive electrode, triangle: aged negative electrode). Reproduced with permission from ref. [83]. Copyright 2017 Carbon Society of Japan

Thus, although templated mesoporous carbons are promising as a negative electrode material for Na-ion batteries, their use in Na-ion capacitors would more effectively utilize their high-rate performance, because capacitors offer high-power operation in contrast to batteries. However, the accompanied huge irreversible capacity is one of the critical issues that must be overcome. In this view, pre-doping process, which is necessary for operation of hybrid capacitors, could prevent the issue of initial irreversible behavior. The performance could be further enhanced by optimizing the pre-doping conditions, as well as the weight balance of the positive and negative electrodes.

Carbon nanotube

A CNT consisting of carbon atoms only, discovered by Dr. Sumio Iijima in 1991 [123], is one of the typical materials in the field of nanotechnology that still attracts the attention of many researchers since CNT is theoretically expected and has been experimentally shown to have excellent electronic and mechanical properties for various applications that thereof will be developed. Carbon nanotubes have a hollow fibrous form that is obtained by cylindrically and seamlessly rolling a graphene sheet roughly categorized into two types based on its structure; one is SWCNT and the other is a multi-walled carbon nanotube (MWCNT). MWCNTs have excellent electroconductivity, and hence have been practically employed as a conductive additive for electrodes in secondary batteries. Although the energy density of an EDLC is theoretically proportional to the solid surface area of the electrode, in a MWCNT where the cylindrical graphene is rolled concentrically, there will be planes where parts of graphene are in contact with one another, and therefore the surface area where electrolyte can reach becomes smaller than that of a SWCNT. From the viewpoint of designing capacitor electrodes, a SWCNT is considered as the ideal form of a CNT since the theoretical surface area of a SWCNT, combining the exterior and interior walls of the tube, is 2630 $m^2 g^{-1}$ which is the same as a monolayer graphene. The application of SWCNTs synthesized by the super growth method (SGCNTs) as a capacitor electrode material boosted and raised up the world largest SWCNTs factory production [18, 49, 124–134]. The mass production of pure SWCNT enabled us to determine the intrinsic properties of the graphenic nanomaterials as capacitor electrodes for the first time and to configure and set up a 1000 F-scale cell [49]. In addition, it has been revealed that pure SWCNT is an excellent binder materials of composite capacitor electrodes on its high conductivity and wide potential window in organic electrolytes. Here, three characteristic properties of SWCNTs are focused upon, their electrochemical behavior in terms of their electronic structure, their wide potential window in organic electrolytes, and their excellent formation ability regardless of the presence of electrochemically active materials, which are all crucial for developing high-performance capacitor devices in commercial use.

Electrochemical behavior of pure SWCNTs

Around the year 2000, early attempts to use CNTs were made in the research field of capacitors [7, 37–40]. However, at that time, the integrity and purity of CNTs could not be satisfactorily controlled, especially for SWCNTs, and the products were inevitably contaminated with metal catalysts and/or amorphous carbons. In order to remove considerable amounts of the metals, the products must be subjected to strong acid treatment. Since the treatment often cleaves the C–C bonds and the tubes themselves, the resultant nanotubes have many defects and edges containing oxygen functional groups, and consequently there is a strong possibility that their structures are far from the ideal ones. Although Shiraishi et al. have studied the properties of purified HiPco nanotubes (commercially available SWCNTs synthesized using a high-pressure carbon monoxide method) in an organic electrolyte and showed that the

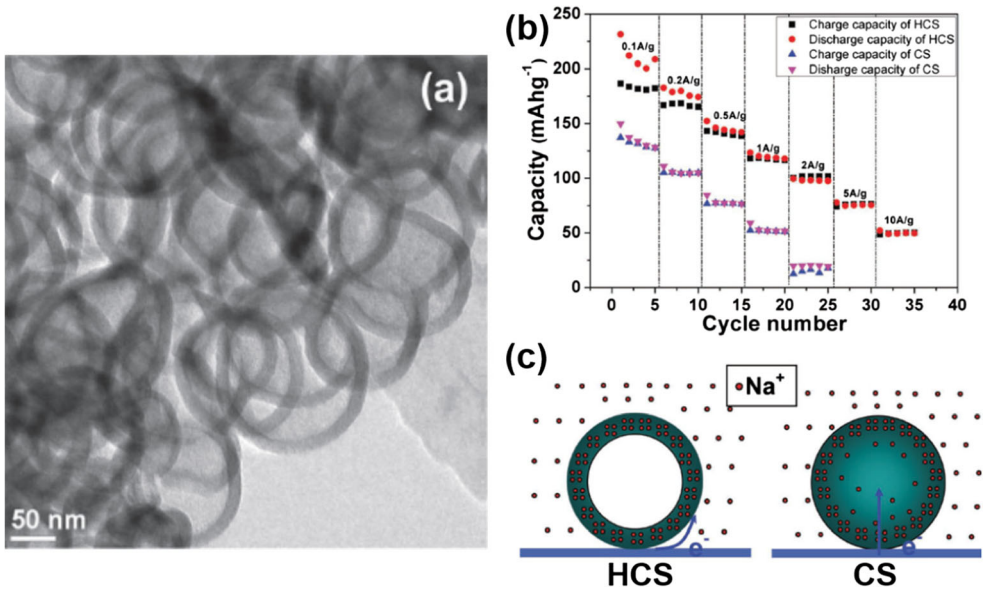

Fig. 6 **a** TEM image of hollow carbon nanospheres, **b** rate performance of hollow carbon nanospheres (HCS) and carbon nanospheres (CS), and **c** schemes of the electrochemical reaction process of HCS and CS. Reproduced with permission from ref. [114]. Copyright 2012 WILEY-VCH Verlag GmbH & Co. KGaA, Weinheim

SWCNTs have a higher specific capacitance per surface area of electrode material than activated carbon fibers, although the mechanism was not clearly identified [135].

A technique called "the super growth method" that enables the manufacture of extremely high purity SWCNTs with an impurity concentration of several hundred ppm or less by weight has been developed by Hata et al. [125] at AIST in 2004. The method employs a silicon or metal substrate with a catalyst-dispersed surface and hydrocarbons as the carbon source, with the SWCNTs being formed from the source on the substrate surface using a chemical vapor deposition process. The method enables the synthesis of a few millimeter-long SWCNTs aligned perpendicularly on the substrate in a short time. The SWCNTs prepared using this method (SG-SWCNTs) can be peeled off the substrate leaving the catalyst on the substrate. In addition, the SG-SWCNTs do not tend to

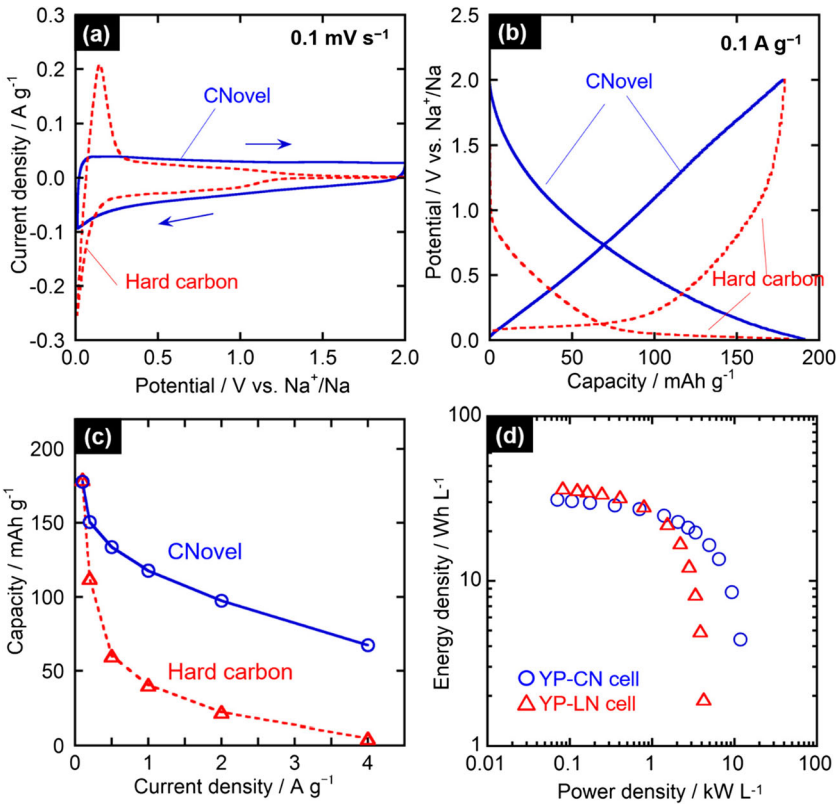

Fig. 7 **a** Cyclic voltammograms, **b** Charge/discharge curves, and **c** the rate performance for CNovel derived from Mg citrate and commercial hard carbons in a potential region of 2.0–0.01 V vs. Na^+/Na in 1 M $NaPF_6$/PC electrolyte [94]. **d** Ragone plots in the full-cell tests (positive electrode: activated carbon, negative electrode: MgO-templated carbon and hard carbon). The electrolyte is a 1 M $NaPF_6$/PC-FEC (2.0 vol%) solution. Reproduced with permission from ref. [96]. Copyright 2016 Elsevier

form bundle-like structures, and instead prefer to grow in a perpendicular alignment on the substrate to form a sheet-shaped object in which the surface area of the closed SWCNTs have a high specific surface area of 1100 $m^2\ g^{-1}$, on the basis of the theoretical value of the outer surface area of SWCNTs, which is 1315 $m^2\ g^{-1}$.

The characteristic properties of pure SWCNTs as a capacitor electrode material, the potential dependent energy storage, are clearly shown in its cyclic voltammograms (CVs) in organic electrolytes. Figure 8a, b shows the CVs of the SG-SWCNT electrode measured in two- and three-electrode cell systems, respectively [126]. The CV of the activated carbon YP-17 was recorded for comparison, in which the current is independent of the cell voltage and hence a rectangular-shape CV is observed, as a result of the typical electric charge accumulation in an electric double-layer, while for the SG-SWCNT system, the current steeply increased with increasing of the voltage (Fig. 8a). This aspect becomes more recognizable in the CV recorded for the SG-SWCNT system in the three-electrode set up, where the profile is butterfly shaped, i.e., there is a symmetric increase and decrease in the current observed for both the positive and negative potentials from the center (ca. − 0.3 V against an Ag^+/Ag reference electrode) resulting in minima currents (Fig. 8b). This indicates that the SWCNT electrode can accumulate electrical charge at a highly polarized potential range. In situ measurements on the electronic conductivity of the SG-SWCNT electrode sheets immersed in an electrolyte resulted in an order of magnitude increase, observed as a V-shape (Fig. 8c), in which the potential of the minimum conductivity (− 0.3 V) matched the potentials associated with the minima currents in the CV plot. It is known that the electronic structure of SWCNTs becomes metallic or semiconducting depending on the chirality, due to the way how the graphene is rolled. The electrochemical behavior of the SG-SWCNT electrode arises from the unique electronic structure of the SWCNTs and can be explained by electrochemical doping of the semiconducting SWCNTs, in which the injection of electrons and holes causes a potential dependence of the electronic conductivity, as shown in Fig. 8c. Due to the above unique electrochemical properties, a capacitor comprising a SWCNT electrode differs in its cell characteristics from the use of one comprising a normal activated carbon electrode. In Fig. 8d, the specific capacitances of the SG-SWCNT and activated carbon electrodes, normalized by their BET surface areas, were plotted against the charging voltage in a two-electrode cell system. While the capacitance of the activated carbon electrode cell is almost constant against the charging voltage, that of the SG-SWCNT electrode cell increases almost proportionally with the voltage [127]. This is one of the cell characteristics unique to SWCNT electrodes [128]. With respect to the specific capacitance per surface area, the SG-SWCNT electrode is far superior to the activated carbon electrode in that the capacitance is 1.5 times or even higher than that of the activated carbon electrode at a charging voltage over 3 V, as shown in Fig. 8d.

Normally, SWCNT synthesis procedures have no chirality-selectivity, and accordingly the product is a mixture of metallic and semiconducting nanotubes. Yamada et al. have reported upon the electrochemical behavior of metallic and semiconducting SWCNTs that were separated using agarose gel chromatography [129]. The CV curves of the metallic and semiconducting SWCNTs separated from the HiPco SWCNTs are shown in Fig. 9a. Although the CV profile of the semiconducting SWCNTs seems to be different from that of the SG-SWCNTs, it showed amphoteric behavior with potential dependence on the current and minima currents at the center potential, while the shape of the CV of the metallic SWCNTs showed less potential dependence. The shape differences of the CV profiles between the SG-SWCNTs, the diameter of which is 3 nm on average with a slightly larger diameter than that of normal SWCNTs, and the separated semiconducting HiPco SWCNTs can be attributed to the difference in the nanotube diameter, which affects the electronic structure of the SWCNTs. It has been more clearly shown by Al-zubaidi et al. [136] that a dumbbell-shaped CV (Fig. 9b) is observed for semiconducting SWCNTs produced using an arc-discharge method and separated through a density gradient ultracentrifugation method. They discussed the relationship between the CV profiles and the density of states for the metallic and semiconducting SWCNTs. Heller et al. carried out simulations on the relationship between the capacitance and the electronic structures of metallic and semiconducting SWCNTs [137]. Regarding the electrochemical doping of SWCNTs, Ruch et al. [138, 139] have observed changes in the Raman intensities and shifts of the D and G^+ bands, as well as in the radial breathing modes (RBMs) during electron and hole injection using in situ Raman spectroscopy, as a function of the electrode potential.

Double-walled carbon nanotubes (DWCNTs), which have different electronic properties from those of SWCNTs due to their coaxial structure, have previously been studied as capacitor electrodes [140–142]. Potential dependent CV profiles similar to those of SWCNTs were reported by Jang et al. [141]. Yamada et al. [18] compared the properties of SWCNTs and DWCNTs prepared using the HiPco method. Although the potential dependence in the CV profiles was not remarkable for the DWCNTs, the sheet conductivity change dependent on the potential was clearly observed, as shown in Fig. 9c. On the other hand, the potential dependence of the specific capacitance is moderate for the DWCNTs, as shown in Fig. 9d and as a result, the difference in the specific capacitance values between the SWCNTs and DWCNTs became large at higher and lower potential ranges apart from the center potential.

Enhancement of the electrode surface area where the electrolyte and ions can come into contact has been attempted for

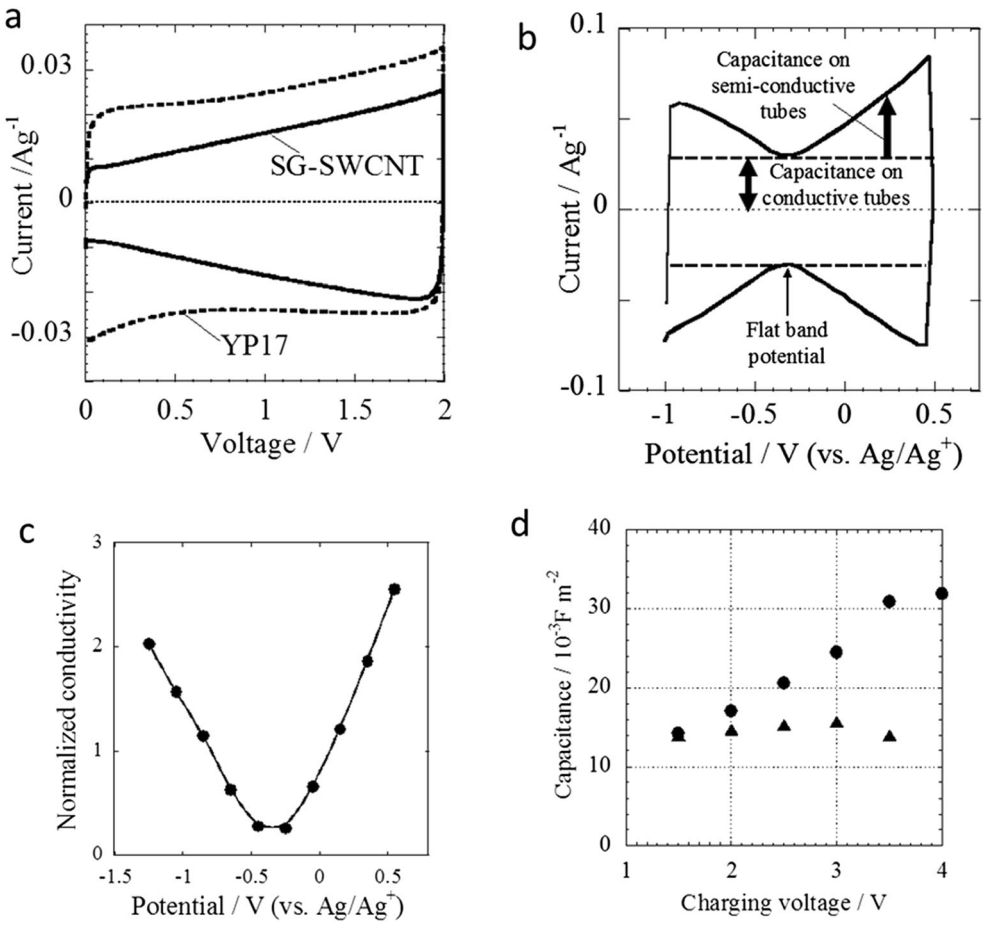

Fig. 8 Cyclic voltammograms in **a** two-electrode and **b** three-electrode cell systems (scan rate: 1 mV/s). Schematic mechanism of capacitance on SG-SWCNTs is shown in Fig. 1b. **c** Potential dependence of in-situ measured electronic conductivity of a densely-pressed SG-SWCNT electrode. **d** Charging-voltage dependence of specific capacitance normalized by BET surface area of electrode materials; black circle SG-SWNT, black triangle YP-17. All measurements were performed in an electrolyte, 1 M tetraethylammonium tetrafluoroborate, $TEABF_4$ in propylene carbonate, PC. Adapted with permission from ref. [126]. Copyright (2008) Elsevier

SWCNTs [130–132]. Since the as-synthesized SG-SWCNTs are basically closed tubes, Hiraoka et al. [131] oxidized the SWCNTs by air and succeeded to increase the surface area up to 2200 $m^2\ g^{-1}$. Yamada et al. [132] studied the hole opening conditions needed to open up the tubes of the SWCNTs and the correlation between the size of the holes and electrolyte intrusion inside of the tubes was discussed in relation to the capacitance. At a charging voltage of 2.5 V, the capacitance enhancement brought about by hole opening at the side of the wall was not adequate in proportion to the increase in the electrode surface area. The potential dependence of the capacitance that occurs because of electrochemical doping indicates that the charge accumulation at the interface between the electrode and the electrolyte is controlled by the charge capacity in the solid side. This means that the capacitance is independent of the electrode surface area, as far as the charge is deficient in the solid electrode side, which is unlike in other carbon materials. As discussed by Yamada et al. [129], optimization of the SWCNT electronic structure by controlling the diameter and/or chirality is considered to be more crucial than enlarging the surface area for SWCNT capacitors in order to maximize the capacitor performance within a limited potential window of the electrolyte from an application viewpoint.

High-performance SWCNT capacitors working at a high operating voltage

Izadi-Najafabadi et al. [133, 134] reported the excellent durability of binder-free SG-SWCNT electrodes. As shown in Fig. 10a, the SG-SWCNT electrode shows a higher specific capacitance upon an increase in the cell voltage. The results shown in Fig. 8d also indicate that pure SWCNT capacitor cells can be operated at a higher voltage of more than 3 V which is higher than that of conventional activated carbon capacitors (Fig. 10b), which normally operate at 2.5–2.7 V. Since the activated carbon electrode is made by mixing polymer binders to connect powdered-activated carbon particles and the auxiliary conducting agent carbon black in order to reduce the contact resistance between the particles, it is possible that these additives can induce the decomposition of all of the components, themselves, activated carbon and electrolytes, under high-voltage conditions. In addition, the additives have no activity for energy storage and hence inhibit any increase in the energy density of the cell system. In contrast, a flexible and highly conductive SWCNT electrode sheet can be obtained without adding a conductive additive or binder, and is thus free from the limitation on the working voltage, which

is restricted by the additive substances. This means that pure SWCNT electrodes, composed of 100% active material, can be used to pursue the intrinsic performance of only the pure electrode in relation only to the electrolyte.

As is shown in the cycle performance results in Fig. 10c, compared to conventional activated carbon electrodes, it was found that sufficiently good durability is maintained for SG-SWCNT electrodes consisting only of pure SWCNTs, even when operated at a high voltage of up to 4 V. In addition to the use of an electrode composition without additives, this is thought to be because there is only an extremely small amount of contaminants present, such as functional groups or metal elements, that may promote the decomposition of the electrolyte solution, on the graphene surface in SG-SWCNT itself. Since the energy density of the capacitor is proportional to the square of the charge voltage, this property is extremely important for increasing the energy density. Due to the increase in the operating voltage up to 4 V and the specific capacitance increasing with an increase in the cell voltage (Fig. 10a), the energy density and the power density of the electrodes reached 94 Wh kg^{-1} (47 Wh L^{-1}) and 210 kW kg^{-1} (105 kW L^{-1}), respectively. Attempts at achieving the practical application of SG-SWCNT capacitors have been undertaken and a trial sample cell working at a maximum voltage of 3.5 V exhibited an energy density of 20 Wh L^{-1} with an excellent durability, estimated to be over 15 years [49]. The large-scale production of SG-SWCNT electrode has enabled actual setup of a 1000 F class EDLC (Fig. 10d), the size of which is suitable for the power regeneration system.

Electrode design based on the formability of CNTs

Numerous reports have detailed the fabrication of capacitors using CNT composites combined with electrochemically active materials for enhancing the electrode performances and/or for flexible and wearable devices, which can be artificially

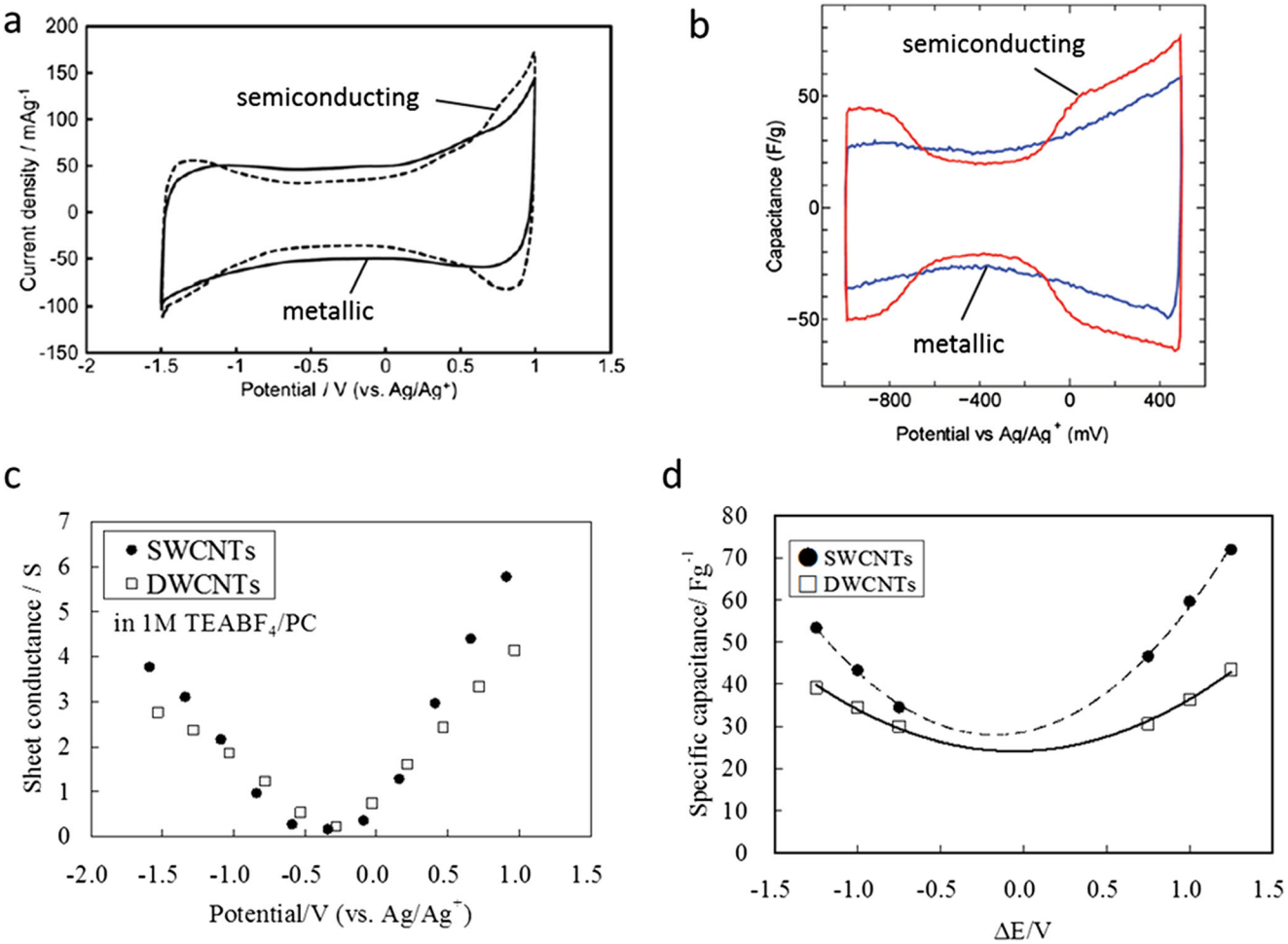

Fig. 9 CVs of metallic and semiconducting SWCNTs, **a** HiPco SWCNTs separated by agarose gel chromatography, adapted with permission from ref. [38], Copyright (2012) Elsevier, and **b** Meijo SWCNTs separated by the density gradient ultracentrifugation method, adapted with permission from ref. [136], Copyright (2012) American Chemical Society. **c** Potential dependence of electronic sheet conductivity on potential and **d** specific capacitance on polarization potential ΔE, deviation from the flat band potential for HiPco SWCNTs and DWCNTs [18]

modified depending on the excellent formability of the CNTs [6, 26, 41, 42, 143–151]. As for the formability of the SWCNT electrode itself, Futaba et al. [152] have reported shape-engineerable and densely packed SG-SWCNT capacitor electrodes. By use of a capillary cohesive force of solution, this method resulted in the formation of a sheet with a density of 0.5 to 0.6 g cm^{-3}, which is 20 times or even larger than the density of a sheet-shaped object as prepared using CVD. The capacitor electrode sheet thus obtained has a high density but exhibits an excellent rate performance compared with that of an activated carbon electrode of the same thickness. The same group studied the design of energy circuits using SWCNTs and lithographically integrated micro-supercapacitors have been reported by Laszczyk et al. [153]

Since it is possible to design various electrochemical capacitors by combining different metals or polymer active materials, pure SWCNTs are excellent binder materials, with durability at high voltage and high capacity. In addition, SWCNTs, with their intrinsic high conductivity and high surface area that are crucial requirements when combining them with other active materials dispersed finely, are outstanding conductive materials. CNTs have been reported as a more effective conductive additive for activated carbon (AC) electrodes than conventionally used acetylene black [154–157]. It is believed that this is due to CNTs providing a uniform conductive network, as the tendency for acetylene black particles to aggregate is detrimental to conductivity. Binder-free composite electrodes in which CNTs act as both a binder and conductive material are a promising option for EDLC applications [143, 146, 158–162] because polymer binders (such as polytetrafluoroethylene) that are normally needed to make robust conventional film electrodes from AC powders create high electrical resistance [162]. As indicated below, a high power density and durability are the remarkable advantages of binder-free composite electrodes made using pure SWCNTs.

Izadi-Najafabadi et al. [163] have reported single-walled carbon nanohorn (SWNH)/nanotube composite electrodes shown in Fig. 11a–d. The composite was assembled by first mixing SWNH particles (80 wt%) with SG-SWCNTs (20 wt%) in dimethylformamide (DMF). After sonication at a moderate power in DMF, the well-dispersed suspension of SWCNT and SWNH particles was poured into a glass dish and then dried. The composite was used to form a supercapacitor electrode with a high maximum power rating (990 kW kg^{-1}; 396 kW L^{-1}), which stemmed from its unique meso–macro pore structure and exhibited durable operation (only a 6.5% decline in capacitance was observed over 100,000 cycles) because of its monolithic chemical composition and mechanical stability.

Kado et al. [17] have demonstrated the superior performance of commercial microporous-activated carbon and SG-SWCNT composite electrodes based on their electrical resistance and stability. In the scanning electron microscope (SEM) image of the AC/SG-SWCNT (80:20 wt%) electrode shown in Fig. 11e–g, it can be obviously observed that the AC particles are distributed and retained in the CNT conductive network, thus leading to a high electronic conductivity. In contrast, the PTFE binder in the conventional AC electrode (AC/AB/PTFE) connects the carbon particles, resulting in a high resistance. The conductivity of the SG-SWCNT electrode was observed to be very high due to its conductive CNT networks, and the AC/SG-SWCNT electrode exhibited a value of 12 S cm^{-1}, which represents more than a tenfold increase in the value compared to that of the conventional AC electrode (0.21 S cm^{-1}). It is considered that there are fewer electrical contact points in the SG-SWCNT composite electrode than in the electrode made from the powdery carbon material. A large difference was observed in the Nyquist plots of the AC impedance spectra of the electrodes. As seen in Fig. 11h, the addition of SG-SWCNTs removed the semicircle in the high-frequency regions and decreased the charge transfer resistance. This charge transfer resistance is mainly attributed to the contact resistance between the electrode and aluminum current collectors. Thus, in addition to improving the electrode conductivity, contact with the etched aluminum foils should be enhanced upon adding SG-SWCNTs. More remarkable is the stability of the composite electrode demonstrated by the results of the accelerated deterioration testing at 60 °C at 3.0 V (Fig. 11i). Here, the ordinate reflects the capacitance retention at given intervals with respect to the initial capacitance, which after 1000 h was higher for the AC/SG-SWCNT electrode (75%) than the AC/AB/PTFE electrode (52%). One possible reason for this result is the electrochemical decomposition of PTFE binders leading to a degradation in the performance of the conventional electrode. Thus, SG-SWCNTs can be effectively used as a binder-free electrode material, i.e., the porous carbon/SG-SWCNT composite electrode was shown to exhibit a lower charge transfer resistance and better cycle-life performance than a conventional electrode. The partial use of pure SWCNTs in electrodes is an effective way of improving EDLC performance, considering that the cost of SWCNTs is still high compared to commercial activated carbons, although SG-SWCNTs are now produced on a mass scale.

Carbons with pseudocapacitive nature

As discussed in the "Introduction" section, introducing the pseudocapacitance is one of the most effective strategies to develop high-energy density capacitors using carbon materials. Although combination with electrochemically active materials such as metal oxides which remarkably enhance the capacitance by redox reactions in aqueous electrolyte is one of typical ways, carbon materials without admixed materials are focused in this section. Since all of carbon materials are composed of graphene layer as a 2D building block, they are able to include the other atoms inside the carbon

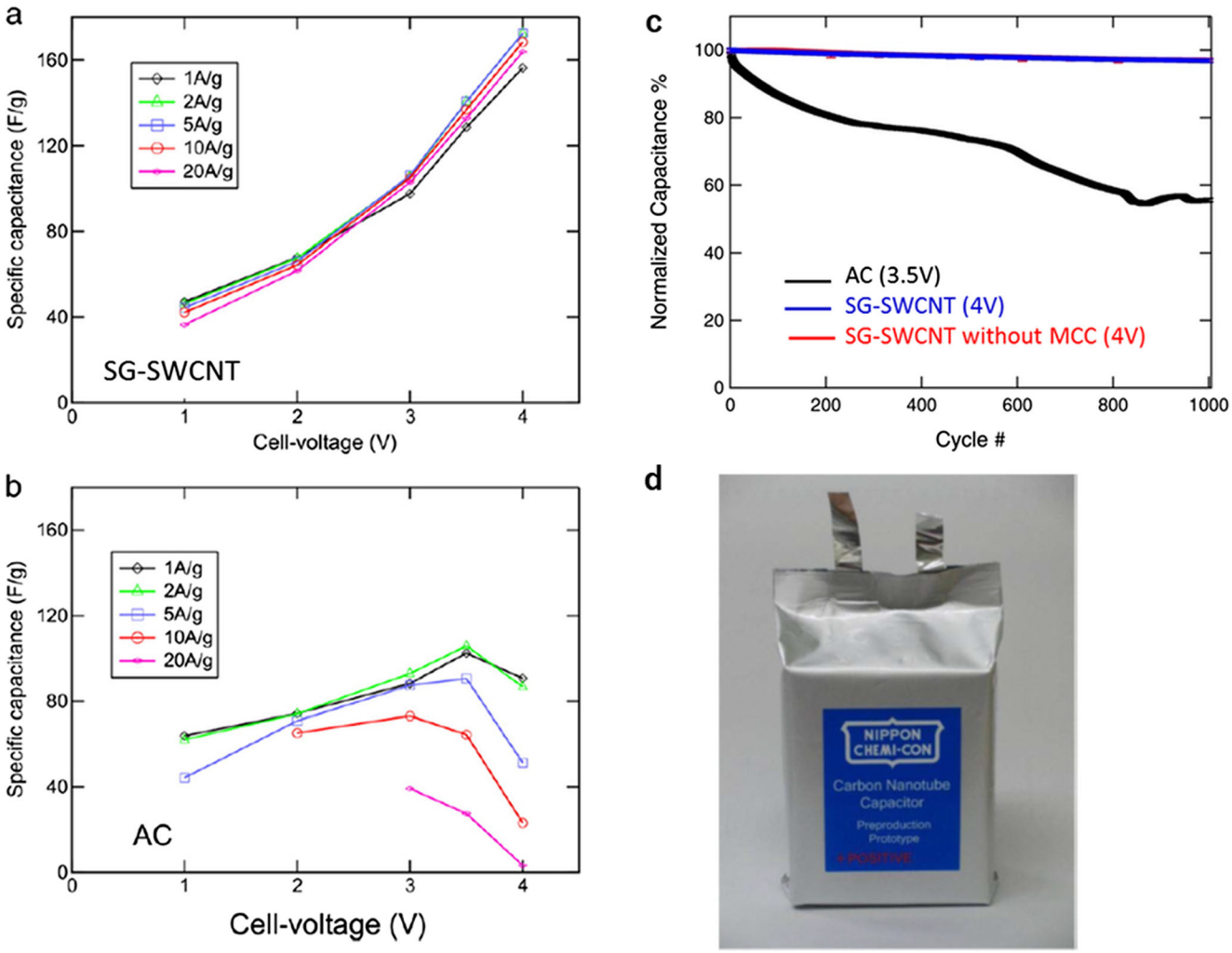

Fig. 10 Specific capacitance of SG-SWCNT and AC determined from galvanostatic discharge curves. Specific capacitance of **a** SWCNT and **b** AC vs. cell-voltage. Adapted with permission from ref. [133]. Copyright (2010) Elsevier. **c** Dynamic Lifetime. Over 1000 cycles of charge/discharge at 1 A g^{-1}, the capacitance of the SG-SWCNT cell with or without metal current collector (MCC) operated at 4 V declines only by 3.6%. In contrast the AC electrode suffers a decline of 46% while operated at 3.5 V [134]. **d** A 1400F SG-SWCNT capacitor cell [49]

hexagonal network and have a possibility to show the interaction through electrons with foreign guest species. In graphene-based materials, while pseudocapacitance is basically due to heteroatom doping, a intercalation-like behavior has been suggested on graphene nanosheet and exfoliated carbon fibers, causing a high capacitance per specific surface area.

Heteroatom-doped carbons

Several researchers have explored doping of heteroatoms such as O [19, 53, 54], N [21, 55–59], B [22, 164], S [165], and P [166] inside the carbon network or at the edge of graphene, that was performed mostly by post thermal treatment of carbons or pyrolysis of heteroatom-containing carbon precursors. Comparing the two methods, use of heteroatom-containing precursors results in a larger amount of heteroatoms in the resultant carbons. In addition, combining this doping method and template method discussed in the former section can realize the heteroatom doping as well as the pore structure control of carbons at the same time. The most studied dopant with the template method is nitrogen using mica and mesoporous silica as templates [20, 167–171]. Kodama et al. have successfully produced N-enriched carbons from quinoline using expandable fluorine mica as a template [20]. Mica is one of layered silicate materials which can accommodate small N-containing organic molecules, such as quinoline and pylidine, in their interlayer spaces. After carbonization, followed by dissolution of mica template, N-enriched carbons can be obtained with a relatively large amount of nitrogen content originating from N-containing organic precursors. The morphology of the carbons reflected the mica template; a very thin circular film was surrounded by the rim having a constant width of ca. 20 nm (Fig. 12a). The obtained N-enriched carbons had a specific surface area of about 80 to 100 m^2 g^{-1} and

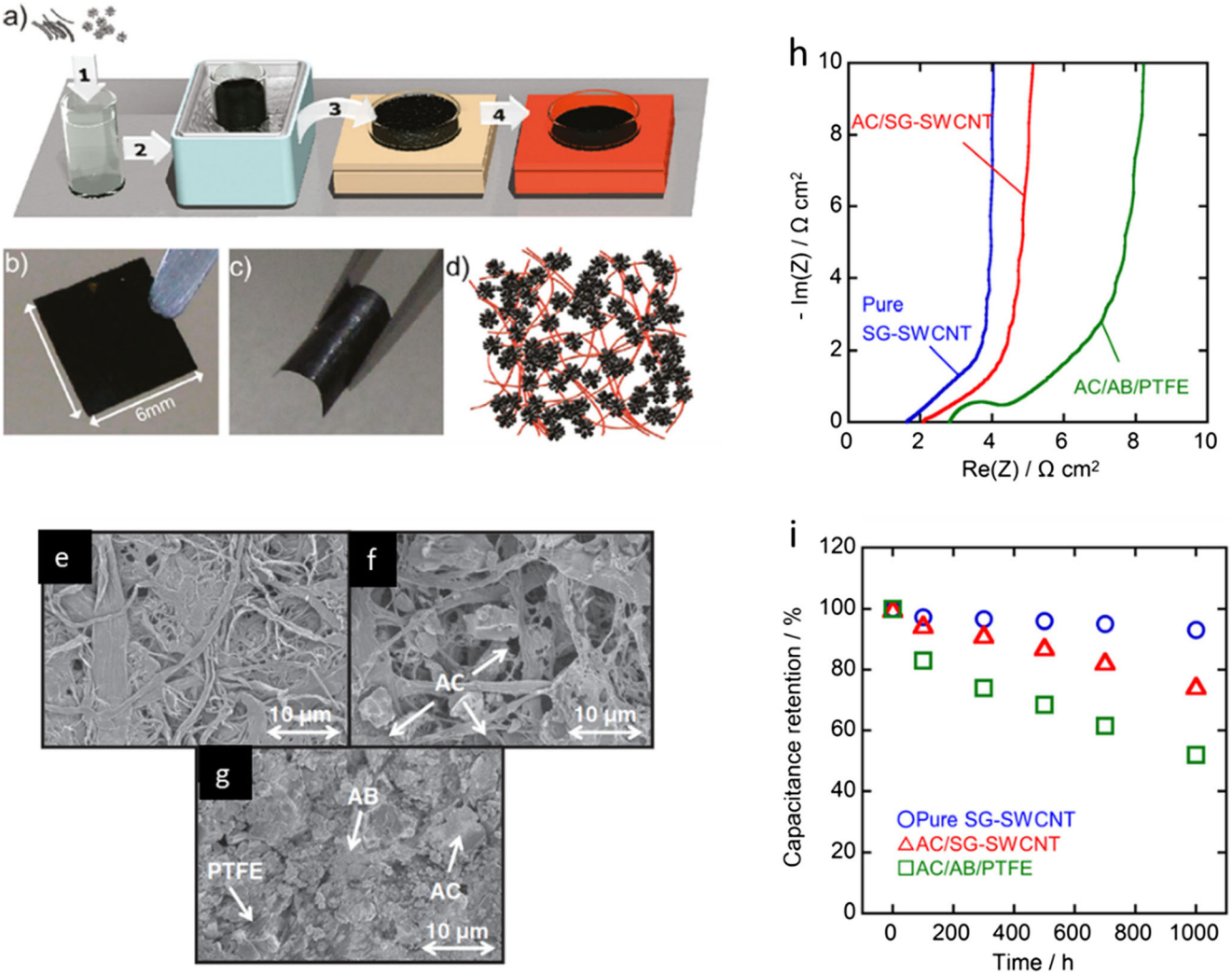

Fig. 11 SWNH/SWNT composite. **a** Fabrication process. **b** Image of a typical SWNH/SWNT composite electrode. **c** Image of the same electrode bent to show its self-supporting capability. **d** Schematic depicting the role of SWNTs as scaffolding for SWNH particles. Adapted with permission from ref. [163]. Copyright (2011) American Chemical Society. SEM images of **e** pure SG-SWCNT, **f** AC/SG-SWCNT, and **g** AC/AB/PTFE electrode [17]. **h** Nyquist plots of the ac impedance spectra and **i** capacitance retention in the accelerated degradation test (60°C, 3.0 V) in 1 M $TEABF_4$/PC for pure SG-SWCNT, AC/SG-SWCNT, and AC/AB/PTFE [17]

a gravimetric capacitance of about 100 to 180 F g^{-1} in 1 M H_2SO_4 electrolyte. This result corresponded to the areal specific capacitance values ranging from 1.2 to 2.2 F m^{-2}, which were tenfold larger than those of conventional activated carbons. Such a unique structure and high capacitance of N-enriched carbons were also observed when the mesoporous silica was used as templates [170, 171]. Figure 12b shows SEM and TEM images of N-enriched mesoporous carbon materials synthesized from quinoline pitch using SBA-15 templates [171]. In the micrographs, a series of straight and aligned mesopores can be clearly observed. The walls of the mesopore structures were composed of N-enriched carbons containing ca. 6 wt% nitrogen and had a significant number of micropores (indicated by N_2 adsorption measurement). Nitrogen-enriched and free carbons showed 250 and 143 F g^{-1} in 1 M H_2SO_4 electrolyte, with the BET surface area of 729 and 595 m^2 g^{-1}, respectively. Clearly, N-enriched carbons showed a higher capacitance than N-free carbons that was made using the same template. Nitrogen content in the carbons can be increased using N-richer carbon precursors, e.g., melamine ($C_3H_6N_6$), with a mica template. Hulicova et al. synthesized the melamine-derived carbons containing 10–40 wt% nitrogen after heat treatments at 650–1000 °C, and exhibited 50–200 F g^{-1} even though the carbons had only 20–440 m^2 g^{-1} specific surface areas [167]. Figure 12c shows a chemical state of nitrogen in melamine-derived carbons; nitrogen existed mainly in the pyridinic, quaternary, and oxidized states. Comparing the spectra of carbons heated at 850 and 1000 °C, the peak owing to quaternary bonding (substituted nitrogen bonded to three neighboring carbon atoms) increased and the peak due to pyridinic bonding (nitrogen located at the outside edges of the carbon rings bonded to two

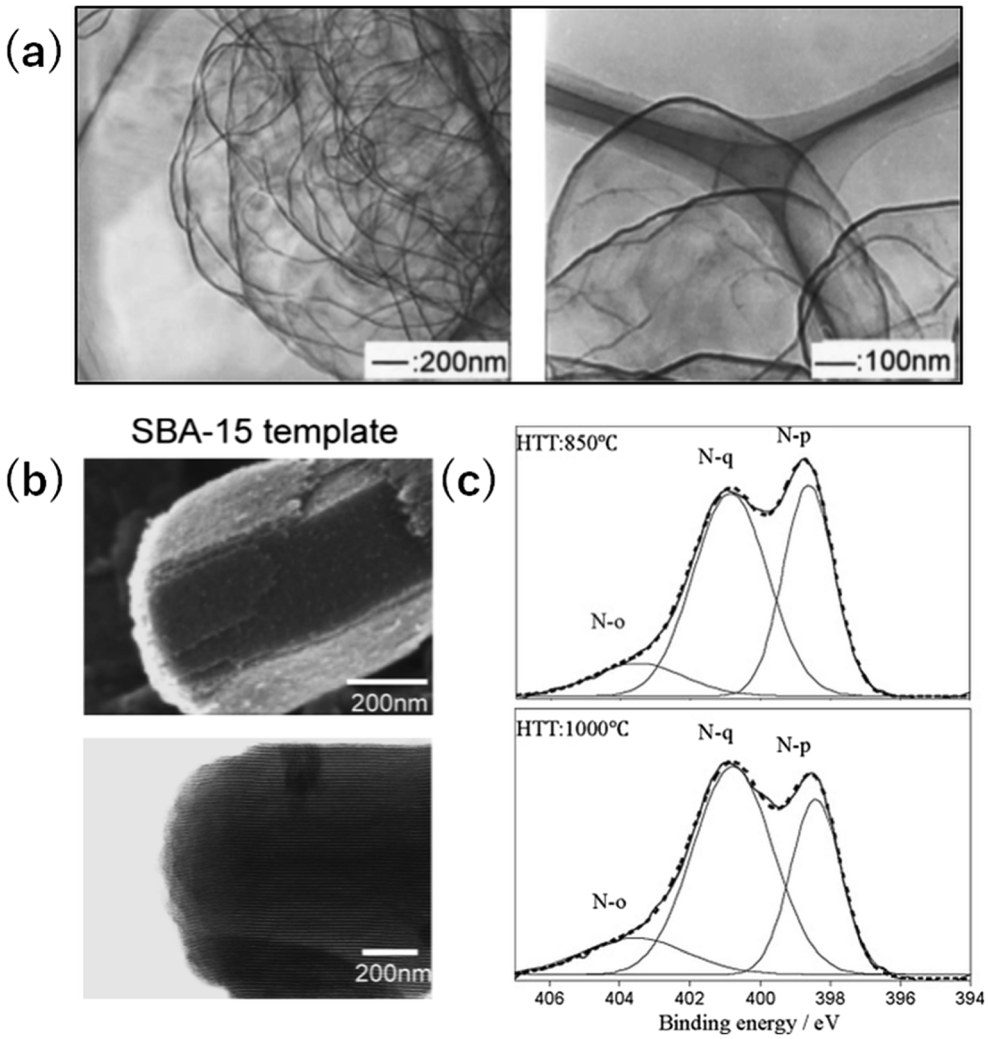

Fig. 12 **a** TEM bright field images of quinoline-derived N-enriched carbons synthesized at 750 °C using expandable fluorine mica template. Reproduced with permission from ref. [20]. Copyright 2004 Elsevier. **b** SEM (upper) and TEM (bottom) images of N-enriched mesoporous carbons synthesized using SBA-15 templates. Reproduced with permission from ref. [171]. Copyright 2013 the Carbon Society of Japan. **c** XPS spectra of N1s core level on the N-enriched carbons synthesized from melamine-intercalated mica at 850 and 1000 °C. N-p, N-q, and N-o denote pyridinic, quaternary, and oxidized chemical state of N bonds, respectively. Reproduced with permission from ref. [167]. Copyright 2005 American Chemical Society

neighboring carbon atoms) decreased with increase in the heating temperature. Nitrogen in the carbon framework would contribute to the fast Faradic reactions between the cations and lone pair electrons in the pyridinic state. However, no clear evidence for any redox reactions were observed in electrochemical measurements such as cyclic voltammetry. Although the mechanism behind the large gravimetric capacitance of carbons with a low surface area was deduced to be some kinds of redox reactions, cyclability has been confirmed up to a few million cycles while maintaining the initial capacitance value.

Apart from the template method, carbonization of melamine foam (used as commercially available cleaning sponges) produced a unique morphology because the obtained carbon foams have resiliency and maintain the shape of original sponges, which enable their use as electrodes without any binders (Fig. 13a) [21]. In addition, the SEM picture shows the entwined branched fibers with a diameter of several micrometers, which is originated from the microstructure of pristine melamine sponge (Fig. 13b). The gravimetric capacitance of the carbon foams reached 240 F g^{-1} at 0.2 A g^{-1} in 1 M H_2SO_4 electrolyte. The BET surface area of the carbon foams was so small that it was regarded less than 1 m^2 g^{-1} from the geometrical surface area. Such a large capacitance value per unit surface area cannot be explained by simple charge accumulation in the electric double layers. This result is, therefore, attributed to the pseudocapacitance involving the nitrogen functionalities. It is also likely that the enhanced wettability relates to the capacitance because of the increased number of hydrophilic sites on the electrode surfaces.

Thus, nitrogen in the carbon network seems to bring about pseudocapacitance of carbon materials for improving energy density, although the mechanism of pseudocapacitance is still not clear. Hulicova et al. [172] reported that pseudocapacitance of N-enriched carbons is significant in acidic and basic media, but not in neutral solutions. In addition, a similar behavior was observed in organic solutions, but the effect was not notable compared to acid or basic aqueous solutions. The nitrogen content in carbonized materials is depending strongly on the type of organic precursors and the

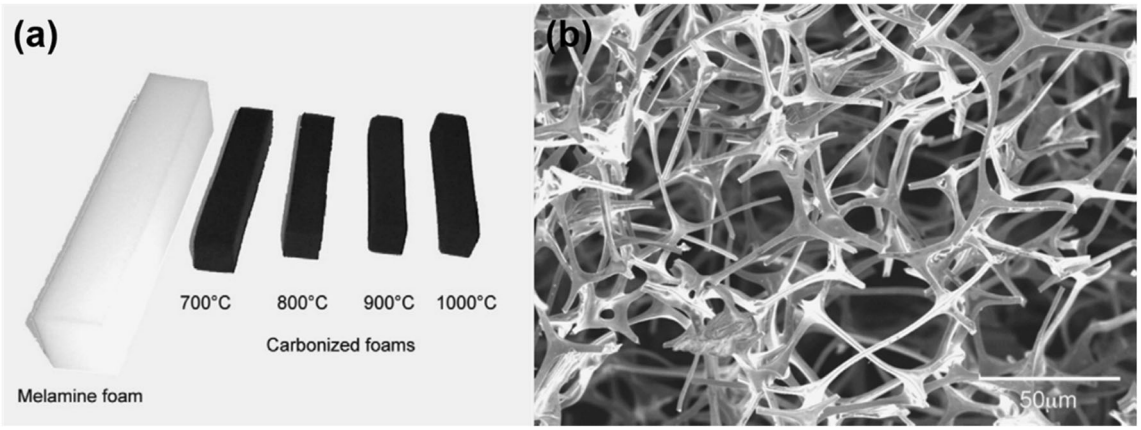

Fig. 13 **a** Photograph of melamine foam (sponge) and its carbonized materials. Dimensions of a pristine melamine foam = 20 × 20 × 110 mm, carbonization temperature = 700–1000 °C. **b** SEM image of carbonized melamine foam at 800 °C. Reproduced with permission from ref. [21]. Copyright 2007 Elsevier

heat treatment temperature. The increase of nitrogen content in carbons tends to reduce the electrical conductivity of materials, thus this could lead the decrease in high power response in actual capacitor devices. In addition to the doping strategy, matching the carbon materials with electrolytes will be one of the key technologies in designing pseudocapacitors.

Graphene nanosheet and exfoliated carbon

In recent years, there has been great interest in graphene-based materials that are new class carbon materials for the electrochemical application [23, 43–48]. Miller et al [43] have demonstrated graphene double-layer capacitor using vertically oriented graphene nanosheets grown directly on metal current collectors. It has been suggested that the capacitor contains pseudocapacitance derived from ion intercalation into exposed edge planes of the graphene structure. In graphene-based materials research, the exfoliated carbon fibers (ExCFs) are one of the pioneers for capacitor electrode materials which show pseudocapacitance by intercalation-like behavior without apparent redox reaction [24, 173–175].

ExCFs were synthesized from carbon fibers (mesophase-pitch- or PAN-based) as a starting material, though many graphene-based materials were prepared from graphite crystal. The intercalation compounds with carbon fibers were obtained by electrolysis in 13 M HNO_3 and then they were rapidly heated to around 1000 °C for a few seconds to achieve exfoliation. The detailed exfoliation behavior of carbon fibers has been reported in several studies [176–178]. The X-ray diffraction patterns of the pristine, electrolyzed, and exfoliated carbon fibers are shown in Fig. 14a. Conventional activated carbon with a low crystallinity is also shown for comparison. The pristine carbon fibers are highly crystalline, exhibiting a sharp diffraction peak with a d-spacing of 0.337 nm (Fig. 14a(i)). After electrooxidation in HNO_3, the diffraction peaks of the graphite structure disappeared and a broad peak at a *d* value of 0.78 nm appeared (Fig. 14a(ii)). According to the chemical analysis of this material, the product of this treatment was determined to be graphite oxide. Subsequently, the graphite oxide was completely decomposed after heat treatment at 1000 °C (Fig. 14a(iii)) and the carbon structure was recovered, although the carbon layer stacking along the *c*-axis was smaller than that observed in pristine carbon fibers, due to the nature of the exfoliation process. SEM observations revealed that individual fibers had formed bundles of thin filaments after the exfoliation, reflecting the fibril texture along the fiber axis. The nitrogen adsorption isotherm for the ExCFs at 77 K showed a developed mesoporous structure, with a BET surface area of around 300 $m^2\ g^{-1}$. Mercury porosimetry measurements were conducted and indicated that the ExCFs have a total pore volume of around 20 $cm^3\ g^{-1}$, which can be reasonably attributed to the meso- and macro-porous regions among the thin filaments.

Extremely large capacitance values reaching 555 and 450 F g^{-1} on ExCFs were observed in the CV and galvanostatic charge–discharge measurements, respectively, when 18 M H_2SO_4 electrolyte with three electrode cells was used. The CV curve slightly deviated from the ideal rectangular shape, but no redox peak was observed. The galvanostatic experiments at low current density resulted in a triangular charge–discharge curve with a linear change in the potential, reflecting the CV curve without any redox peaks. Galvanostatic cycling at a high current density (500 mA g^{-1}) in 18 M H_2SO_4 was measured as being stable for more than 7000 cycles. Figure 14b shows the areal-specific capacitance of the ExCFs and activated carbon fibers (ACFs), plotted against the H_2SO_4 electrolyte concentration. The capacitance value for the ExCFs was observed to increase gradually upon an increase in the concentration up to 10 M then suddenly jumped to an extremely large value in the higher concentration region, reaching about 1.4 F m^{-2} (450 F g^{-1}). However, the capacitance value of the ACFs did not show any trend upon a change in the electrolyte concentration and maintained an

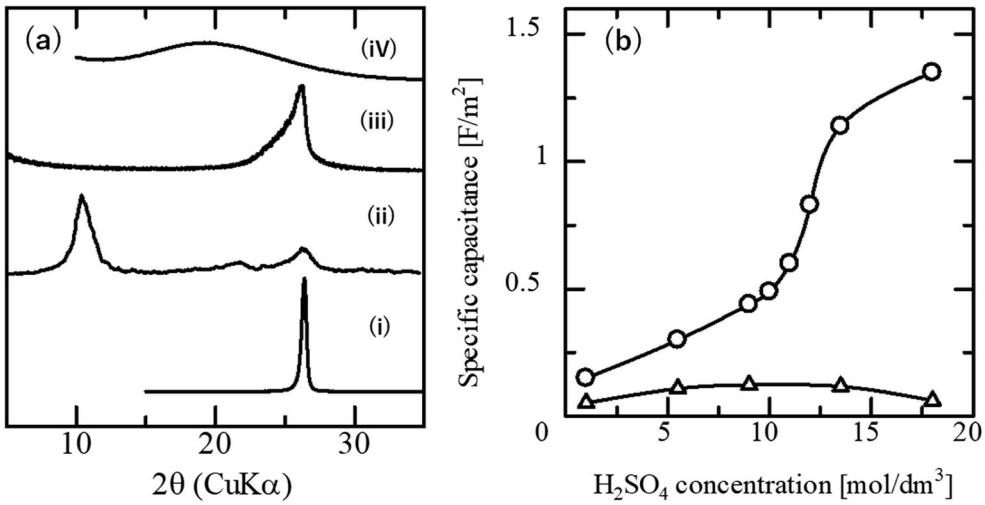

Fig. 14 **a** X-ray diffraction patterns of carbon fiber: (i) pristine mesophase-based graphitized carbon fiber, (ii) electrolyzed in 13 M HNO_3 forming intercalation compound, (iii) exfoliated (heat-treated at 1000°C for 5 s), and (iv) conventional activated carbon. Reproduced with permission from ref. [173]. Copyright 2003 Elsevier. **b** Dependence of areal specific capacitance of ExCF (circle) and activated carbon fiber (triangle) on the concentration of H_2SO_4 electrolyte. Reproduced with permission from ref. [24]. Copyright 2004 Elsevier

approximately constant, small value of about 0.1 F m^{-2}. Since the capacitance value of the ExCFs in concentrated H_2SO_4 is considerably large compared with the reported value of conventional carbon materials, the value for ExCFs obtained here cannot be explained only by the electric double-layer capacitance, the pseudocapacitance due to intercalation of H_2SO_4 must be also considered. In the case of exfoliated natural graphite (ExNG) with the higher crystallinity which showed a similar trend, abnormally large capacitances were obtained in 12 and 18 M solutions, and a distinct intercalation reaction of H_2SO_4 molecules into the graphite interlayer (stage structure) was identified. This observation indicates that the enhancement of the specific capacitance of ExCFs with concentrated electrolyte is not associated with the formation of a stage structure caused by the intercalation reaction, although there may be some strong interactions between the carbon layers and the H_2SO_4 molecules. The lack of stage structure formation in the ExCFs may be due to the lower crystallinity and more distorted nature of its structure compared to that of graphite. The capacitive performance of the ExCFs is better than that of ExNG, because of no formation of the stage structure involving a volume change in the electrode and subsequent electrode collapse at short cycling times. In addition, the enhanced rate performance of ExCFs could be also expected, if the surface reaction makes a major contribution to the pseudo-capacitance.

Thus, the pseudocapacitive behavior of graphene and related materials (including ExCFs) could be attributed to the enhanced adsorption of ions, in other words the interactions between the ions and basal planes [179] or edge sites (intercalation [24, 43, 173, 175] and functional groups [180, 181]). Because both the intercalation reaction into interlayer spaces and the ion adsorption on basal planes result in the charge transfer between guest species and π-electron of graphene sheet, the design of 3D architecture of graphene-related materials with suppressed agglomeration is being the current topic. The system composed of safe guest species with graphenic materials is necessary to apply for actual devices, though high concentration of sulfuric acid with ExCF indicates the basic concepts.

Summary and future perspectives

In this review, we have highlighted the design and synthesis of a variety of advanced carbons as primary electrode materials for electrochemical capacitors. The template method for highly ordered carbon pore structures has become a powerful tool to enhance ion transfer in the pores, which contributes to high-power performance. To improve the energy density, it is possible to develop pseudocapacitors or hybrid capacitors based on carbons without any admixed materials. For instance, the reactions between cations and lone pair electrons in N-doped carbons and the intercalation (-like) behaviors of ions (SO_4^{2-}, Li^+, Na^+, etc.) can be utilized as redox reactions for high-energy density capacitors. It is challenging to establish fast and reversible reactions without any loss of desired EDLC features, such as high-power, long durability, and high reliability. In addition, as indicated by the research on SWCNTs, not only improving the specific capacitance but also enhancing the working cell voltage in relation to the properties of the electrolyte used are keys to enhancing the energy density of capacitor devices.

Recently, the most popular research topic in carbon electrode materials has been graphene-based materials (including composite electrodes with other active materials) for application to electrochemical capacitors (and other energy devices). In addition to the structural design of carbon materials, comprehensive understanding of the relationship between the intrinsic nature of carbon solids (of which the graphene layers are basically composed of sp^2 carbon atoms) and the properties of electrolytes is not only basic but also crucial for developing commercial capacitor devices using any carbon

material. For example, pure SWCNT has been proven to be an excellent binder of composite capacitor electrodes, not diminishing the cell performance (unlike polymer binders), because the material has high electrical conductivity and a wide potential window in organic electrolytes, as demonstrated by its EDLC performance. Thus, study on graphene as a carbon family reminds us again that many of the superior characteristics of CNTs come from the nature of hexagonal carbon networks with sp^2 hybridization. In line with this consideration, various types of carbon materials, including advanced and conventional carbons with different morphology, microtexture, porous structure, surface, and edge chemistry, will be explored with the help of graphene science to develop future capacitor electrode materials.

Acknowledgements This work was supported by the NEDO (New Energy and Industrial Technology Development Organization) Energy Innovation Program "Development of the carbon nanotube capacitor" (FY 2006–2010), and the NEDO R&D program for the Practical Utilization of Nanotechnology and Advanced Materials "Development of the aqueous electrochemical supercapacitor by hybrid nanocarbon electrode" (FY 2008–2011). We are grateful to the people who engaged in this joint research between Oita University, Toyo Tanso Co., Ltd., NEC Tokin Corporation and the Nippon Chemi-Con Corporation.

References

1. International Energy Agency (2018) World energy outlook 2017. OECD/IEA, Paris
2. Miller JR, Simon P (2008) Science 321(5889):651–652
3. Conway BE (1999) Electrochemical supercapacitors: scientific fundamentals and technological applications. Kluwer Academic/Plenum Publisher, New York
4. Kötz R, Carlen M (2000) Electrochim Acta 45(15-16):2483–2498
5. Miller JR (2016) J Power Sources 326:726–735
6. Inagaki M, Konno H, Tanaike O (2010) J Power Sources 195(24):7880–7903
7. Frackowiak E, Béguin F (2001) Carbon 39(6):937–950
8. Gryglewicz G, Machnikowski J, Grabowska E, Lota G, Frackowiak E (2005) Electrochim Acta 50(5):1197–1206
9. Raymundo-Piñero E, Kierzek K, Machnikowski J, Beguin F (2006) Carbon 44(12):2498–2507
10. Shiraishi S (2013) Bol Grupo Español Carbón 28:18–24
11. Fuertes AB, Lota G, Centeno TA, Frackowiak E (2005) Electrochim Acta 50(14):2799–2805
12. Nishihara H, Itoi H, Kogure T, Hou P-X, Touhara H, Okino F, Kyotani T (2009) Chem Eur J 15(21):5355–5363
13. Soneda Y, Kodama M (2013) Electrochemistry 81(10):845–848
14. Fang B, Wei YZ, Maruyama K, Kumagai M (2005) J Appl Electrochem 35(3):229–233
15. Lin C, Ritter JA, Popov BN (1999) J Electrochem Soc 146(10):3639–3643
16. Chmiola J, Yushin G, Gogotsi Y, Portet C, Simon P, Taberna PL (2006) Science 313(5794):1760–1763
17. Kado Y, Imoto K, Soneda Y, Yoshizawa N, Horii D, Suematsu S (2016) J Electrochem Soc 163(8):A1753–A1758
18. Yamada Y, Kimizuka O, Tanaike O, Machida K, Suematsu S, Tamamitsu K, Saeki S, Hatori H (2009) Electrochem Solid-State Lett 12(3):K14–K16
19. Raymundo-Piñero E, Leroux F, Béguin F (2006) Adv Mater 18(14):1877–1882
20. Kodama M, Yamashita J, Soneda Y, Hatori H, Nishimura S, Kamegawa K (2004) Mater Sci Eng B 108(1-2):156–161
21. Kodama M, Yamashita J, Soneda Y, Hatori H, Kamegawa K (2007) Carbon 45(5):1105–1107
22. Wang D-W, Li F, Chen Z^G, Lu GQ, Cheng H-M (2008) Chem Mater 20(22):7195–7200
23. Stoller MD, Park S, Zhu Y, An J, Ruoff RS (2008) Nano Lett 8(10):3498–3502
24. Soneda Y, Toyoda M, Tani Y, Yamashita J, Kodama M, Hatori H, Inagaki M (2004) J Phys Chem Solids 65(2-3):219–222
25. Simon P, Gogotsi Y (2008) Nat Mater 7(11):845–854
26. Béguin F, Presser V, Balducci A, Frackowiak E (2014) Adv Mater 26(14):2219–2251
27. Wang L, Toyoda M, Inagaki M (2008) New Carbon Mater 23(2):111–115
28. Salitra G, Soffer A, Eliad L, Cohen Y, Aurbach D (2000) J Electrochem Soc 147(7):2486–2493
29. Largeot C, Portet C, Chmiola J, Taberna PL, Gogotsi Y, Simon P (2008) J Am Chem Soc 130(9):2730–2731
30. Persons R (1990) Chem Rev 90(5):813–826
31. Pandolfo AG, Hollenkamp AH (2006) J Power Sources 157(1):11–27
32. Xie Y, Kocaefe D, Chen C, Kocaefe Y (2016) J Nanomater 2016:2302595
33. Inagaki M, Toyoda M, Soneda Y, Tsujimura S, Morishita T (2016) Carbon 107:448–473
34. Yoon SH, Lee J, Hyeon T, Oh SM (2002) J Electrochem Soc 147:2507–2512
35. Nishihara H, Kyotani T (2012) Adv Mater 24(33):4473–4498
36. Morishita T, Tsumura T, Toyoda M, Przepiórski J, Morawski AW, Konno H, Inagaki M (2010) Carbon 48(10):2690–2707
37. Niu CM, Sichel EK, Hoch R, Moy D, Tennent H (1997) Appl Phys Lett 70(11):1480–1482
38. Frackowiak E, Metenier K, Bertagna V, Beguin F (2000) Appl Phys Lett 77(15):2421–2423
39. Barisci JN, Wallace GG, Baughman RH (2000) J Electrochem Soc 147(12):4580–4583
40. An KH, Kim WS, Park YS, Choi YC, Lee SM, Chung DC, Bae DJ, Lim SC, Lee YH (2001) Adv Mater 13(7):497–500
41. Lota G, Fic K, Frackowiak E (2011) Energy Environ Sci 4(5):1592–1605
42. Chen T, Dai LM (2013) Mater Today 16(7-8):272–280
43. Miller JR, Outlaw RA, Hollowa BC (2010) Science 329(5999):1637–1639
44. Vivekchand SRC, Rout CS, Subrahmanyam KS, Govindaraj A, Rao CNR (2008) J Chem Sci 120(1):9–13
45. Huang Y, Liang J, Chen Y (2012) Small 8(12):1805–1834
46. Lemine AS, Zagho MM, Altahtamouni TM, Bensalah N (2018) Int J Energy Res 42(14):4284–4300. https://doi.org/10.1002/er.4170
47. Chen J, Li C, Shi G (2013) J Phys Chem Lett 4(8):1244–1253
48. Raccichini R, Varzi A, Passerini S, Scrosati B (2015) Nat Mater 14(3):271–279
49. NEDO Carbon Nanotube Capacitor Development Project (2011) Evaluation report http://www.nedo.go.jp/content/100433173.pdf. Accessed 1 Oct 2018
50. Naoi K, Simon P (2008) Electrochem Soc Interface 17:34–37
51. Conway BE (1991) J Electrochem Soc 138(6):1539–1548
52. Conway BE, Birss V, Wojtowicz J (1997) J Power Sources 66(1-2):1–14
53. Oda H, Yamashita A, Minoura S, Okamoto M, Morimoto T (2006) J Power Sources 158(2):1510–1516

54. Hsieh C, Teng H (2002) Carbon 40(5):667–674
55. Frackowiak E, Lota G, Machnikowski J, Guterl CV, Béguin F (2006) Electrochim Acta 51(11):2209–2214
56. Inagaki M, Toyoda M, Soneda Y, Morishita T (2018) Carbon 132: 104–140
57. Lota G, Grzyb B, Machnikowska H, Machnikowski J, Frackowiak E (2005) Chem Phys Lett 404(1-3):53–58
58. Hulicova-Jurcakova D, Seredych M, Lu GQ, Bandosz TJ (2009) Adv Funct Mat 19(3):438–447
59. Sahoo MK, Gogoi P, Rajeshkhanna G, Chilukuri SV, Rao GR (2017) Appl Surf Sci 418:40–48
60. Ryu KS, Kim KM, Park NG, Park YJ, Chang SH (2002) J Power Sources 103(2):305–309
61. Rudge A, Davey J, Raistrick I, Gottesfeld S, Ferrais JP (1994) J Power Sources 47(1-2):89–107
62. Laforgue A, Simon P, Sarrazin C, Fauvarque JF (1999) J Power Sources 80(1-2):142–148
63. Toupin M, Brousse T, Bélanger D (2004) Chem Mater 16(16): 3184–3190
64. Liu KC, Anderson MA (1996) J Electrochem Soc 143(1):124–130
65. Zheng JP, Cygan PJ, Jow TR (1995) J Electrochem Soc 142(8): 2699–2703
66. Meher SK, Rao GR (2011) J Phys Chem C 115(31):15646–15654
67. Naoi K, Naoi W, Aoyagi S, Miyamoto J, Kamino T (2013) Acc Chem Res 46(5):1075–1083
68. Fisher RA, Watt MR, Readya WJ (2013) ECS J Solid State Sci Technol 2(10):M3170–M3177
69. Kyotani T, Tsai LF, Tomita A (1995) Chem Mater 7(8):1427–1428
70. Ahn HJ, Sohn JI, Kim YS, Shim HS, Kim WB (2006) Electrochem Commun 8(4):513–516
71. Vix-Guterl C, Frackowiak E, Jurewicz K, Friebe M, Parmentier J, Beguin F (2005) Carbon 43(6):1293–1302
72. Li L, Song H, Chen X (2006) Electrochim Acta 51(26):5715–5720
73. Liu HY, Wang KP, Teng H (2005) Carbon 43(3):559–566
74. Nishihara H, Yang QH, Hou PX, Unno M, Yamauchi S, Saito R, Paredes JI, Martinez-Alonso A, Tascon JMD, Sato Y, Terauchi M, Kyotani T (2009) Carbon 47(5):1220–1230
75. Moriguchi I, Nakahara F, Furukawa H, Yamada H, Kudo T (2004) Electrochem Solid-State Lett 7(8):A221–A223
76. Morishita T, Ishihara K, Kato M, Inagaki M (2007) Carbon 45(1): 209–211
77. Inagaki M, Kato M, Morishita T, Morita K, Mizuuchi K (2007) Carbon 45(5):1121–1124
78. Nakazono T, Morishita T (2016) KONA Powder Particle J 33(0): 333–339
79. Morishita T, Ishihara K, Kato M, Tsumura T, Inagaki M (2007) TANSO 2007(226):19–24
80. Kado Y, Imoto K, Soneda Y, Yoshizawa N (2014) J Power Sources 271:377–381
81. Kado Y, Soneda Y, Yoshizawa N (2015) J Power Sources 276: 176–180
82. Kado Y, Imoto K, Soneda Y, Yoshizawa N (2016) J Power Sources 305:128–133
83. Kado Y, Soneda Y (2017) TANSO 280:182–187
84. Mitani S, Lee SI, Yoon SH, Korai Y, Mochida I (2004) J Power Sources 133(2):298–301
85. Mitani S, Lee SI, Saito K, Korai Y, Mochida I (2006) Electrochim Acta 51(25):5487–5493
86. Sevilla M, Álvarez S, Centeno T, Fuertes A, Stoeckli F (2007) Electrochim Acta 52(9):3207–3215
87. Centeno TA, Stoeckli F (2006) Electrochim Acta 52(2):560–566
88. Ishimoto S, Asakawa Y, Shinya M, Naoi K (2009) J Electrochem Soc 156(7):A563–A571
89. Ruch PW, Cericola D, Foelske A, Kötz R, Wakaun A (2010) Electrochim Acta 55(7):2352–2357
90. Shiraishi S (2012) Key Eng Mater 497:80–86
91. Muroi S, Iida D, Tsuchikawa T, Yabuuchi N, Horikoshi R, Hosono N, Komatsu D, Komaba S (2015) Electrochemistry 83(8):609–618
92. Tokita M, Yoshimoto N, Fujii K, Morita M (2016) Electrochim Acta 209:210–218
93. Frackowiak E, Béguin F (2002) Carbon 40(10):1775–1787
94. Kado Y, Soneda Y, Yoshizawa N (2015) ECS Electrochem Lett 4: A22–A23
95. Kado Y, Soneda Y, Yoshizawa N (2015) J Appl Electrochem 45(3):273–280
96. Kado Y, Soneda Y (2016) J Phys Chem Solids 99:167–172
97. Cazorla-Amorós D, Lozano-Castelló D, Morallón E, Bleda-Marínez MJ, Linares-Solano A, Shiraishi S (2010) Carbon 48(5):1451–1456
98. Wang J, Polleux J, Lim J, Dunn B (2007) J Phys Chem C 111(40): 14925–14931
99. Brezesinski T, Wang J, Tolbert SH, Dunn B (2010) Nat Mater 9(2):146–151
100. Brezesinski K, Haetge J, Wang J, Mascotto S, Reitz C, Rein S, Tolbert SH, Perlich J, Dunn B, Brezesinski T (2011) Small 7(3): 407–414
101. Karthikeyan K, Amaresh S, Lee SN, Aravindan V, Lee YS (2014) Chem Asian J 9(3):852–857
102. Frackowiak E, Gautier S, Gaucher H, Bonnamy S, Béguin F (1999) Carbon 37(1):61–69
103. Nishi Y (2001) J Power Sources 100(1-2):101–106
104. Tarascon JM, Armand M (2001) Nature 414(6861):359–367
105. Armand M, Tarascon JM (2008) Nature 451(7179):652–657
106. Palacin MR (2009) Chem Soc Rev 38(9):2565–2575
107. Kim SW, Seo DH, Ma X, Ceder G, Kang K (2012) Adv Energy Mater 2(7):710–721
108. Slater MD, Kim D, Lee E, Johnson CS (2013) Adv Funct Mater 23(8):947–958
109. Clarke FW, Washington HS (1922) Proc Natl Acad Sci U S A 8(5):108–115
110. Stevens DA, Dahn JR (2000) J Electrochem Soc 147(4):1271–1273
111. Alcántara R, Lavela P, Ortiz JF, Tirado JL (2005) Electrochem Solid-State Lett 8(4):A222–A225
112. Komaba S, Murata W, Ishikawa T, Yabuuchi N, Ozeki T, Nakayama T, Ogata A, Gotoh K, Fujiwara K (2011) Adv Funct Mater 21(20):3859–3867
113. Wenzel A, Hara T, Janek J, Adelhelm P (2011) Energy Environ Sci 4(9):3342–3345
114. Tang K, Fu L, White RJ, Yu L, Titirici M-M, Antonietti M, Maier J (2012) Adv Energy Mater 2(7):873–877
115. Cao Y, Xiao L, Sushko ML, Wang W, Schwenzer B, Xiao J, Nie Z, Saraf LV, Yang Z, Liu J (2012) Nano Lett 12(7):3783–3787
116. Kuratani K, Yao M, Senoh H, Takeichi N, Sakai T, Kiyobayashi T (2012) Electrochim Acta 76:320–325
117. Shao Y, Xiao J, Wang W, Engelhard M, Chen X, Nie Z, Gu M, Saraf LV, Exarhos G, Zhang J-G, Liu J (2013) Nano Lett 13(8): 3909–3914
118. Lotfabad EM, Kalisvaart P, Kohandehghan A, Karpuzov D, Mitlin D (2014) J Mater Chem A 2(46):19685–19695
119. Han P, Han X, Yao J, Zhang L, Cao X, Huang C, Cui G (2015) J Power Sources 297:457–463
120. Guan Z, Liu H, Xu B, Hao X, Wang Z, Chen L (2015) J Mater Chem A 3(15):7849–7854
121. Liu H, Jia M, Sun N, Cao B, Chen R, Zhu Q, Wu F, Qiao N, Xu B (2015) ACS Appl Mater Interfaces 7(49):27124–27130
122. Hasegawa G, Kanamori K, Kannari N, Ozaki J, Nakanishi K, Abe T (2016) J Power Sources 318:41–48

123. Iijima S (1991) Nature 345:56–58
124. Hatori H, Tanaike O, Soneda Y, Kodama M (2014) Synthesiology 6:222–231
125. Hata K, Futaba DN, Mizuno K, Namai T, Yumura M, Iijima S (2004) Science 306(5700):1362–1364
126. Kimizuka O, Tanaike O, Yamashita J, Hiraoka T, Futaba DN, Hata K, Machida K, Suematsu S, Tamamitsu K, Saeki S, Yamada Y, Hatori H (2008) Carbon 46(14):1999–2001
127. Tanaike O, Futaba DN, Hata K, Hatori H (2009) Carbon Lett 10(2):90–93
128. Tanaike O, Hatori H, Hata K (2011), a) JP PAT 4706066, 2011, b) US PAT 8072733, 2011
129. Yamada Y, Tanaka T, Machida K, Suematsu S, Tamamitsu K, Kataura H, Hatori H (2012) Carbon 50(3):1422–1424
130. Tanaike O, Kimizuka O, Yoshizawa N, Yamada K, Wang XQ, Hatori H, Toyoda M (2009) Electrochem Commun 11(7):1441–1444
131. Hiraoka T, Izadi-Najafabadi A, Yamada T, Futaba DN, Yasuda S, Tanaike O, Hatori H, Yumura M, Iijima S, Hata K (2010) Adv Funct Mater 20(3):422–428
132. Yamada Y, Kimizuka O, Machida K, Suematsu S, Tamamitsu K, Saeki S, Yoshizawa N, Tanaike O, Yamashita J, Don F, Hata K, Hatori H (2010) Energy Fuel 24(6):3373–3377
133. Izadi-Najafabadi A, Yamada T, Futaba DN, Hatori H, Iijima S, Hata K (2010) Electrochem Commun 12(12):1678–1681
134. Izadi-Najafabadi A, Yasuda S, Kobashi K, Yamada T, Futaba DN, Hatori H, Yumura M, Iijima S, Hata K (2010) Adv Mater 22(35):E235–E241
135. Shiraishi S, Kurihara H, Okabe K, Hulicova D, Oya A (2002) Electrochem Commun 4(7):593–598
136. Al-zubaidi A, Inoue T, Matsushita T, Ishii Y, Hashimoto T, Kawasaki S (2012) J Phys Chem C 116(14):7681–7686
137. Heller I, Kong J, Williams KA, Dekker C, Lemay SG (2006) J Am Chem Soc 128(22):7353–7359
138. Ruch PW, Hardwick LJ, Hahn M, Foelske A, Koetz R, Wokaun A (2009) Carbon 47(1):38–52
139. Ruch PW, Kótz R, Wokaun A (2009) Electrochim Acta 54(19):4451–4458
140. Honda Y, Takeshige M, Shiozaki H, Kitamura T, Yoshikawa K, Chakrabarti S, Suekane O, Pan L, Nakayama Y, Yamagata M, Ishikawa M (2008) J Power Sources 185(2):1580–1584
141. Jang IY, Muramatsu H, Park KC, Kim YJ, Endo M (2009) Electrochem Commun 11(4):719–723
142. Kim YJ, Kim YA, Chino T, Suezaki H, Endo M, Dresselhaus MS (2006) Small 2(3):339–345
143. Xu G, Zheng C, Zhang Q, Huang J, Zhao M, Nie J, Wang X, Wei F (2011) Nano Res 4(9):870–881
144. Ghosh A, Lee YH (2012) ChemSusChem 5(3):480–499
145. Zhang JT, Zhao XS (2012) ChemSusChem 5(5):818–841
146. Chen H, Di J, Jin Y, Chen M, Tian J, Li Q (2013) J Power Sources 237:325–331
147. Yan J, Wang Q, Wei T, Fan ZJ (2014) Adv Energy Mater 4(4):1300816
148. Mai LQ, Tian XC, Xu X, Chang L, Xu L (2014) Chem Rev 114(23):11828–11862
149. Vlad A, Singh N, Galande C, Ajayan PM (2015) Adv Energy Mater 5(19):1402115
150. Yang ZB, Ren J, Zhang ZT, Chen XL, Guan GZ, Qin LB, Zhang Y, Peng HS (2015) Chem Rev 115(11):5159–5223
151. Liu LL, Niu ZQ, Chen J (2016) Chem Soc Rev 45(15):4340–4363
152. Futaba DN, Hata K, Yamada T, Hiraoka T, Hayamizu Y, Kakudate Y, Tanaike O, Hatori H, Yumura M, Iijima S (2006) Nature Mater 5(12):987–994
153. Laszczyk KU, Kobashi K, Sakurai S, Sekiguchi A, Futaba DN, Yamada T, Hata K (2015) Adv Energy Mater 5(18):1500741
154. Taberna P-L, Chevallier G, Simon P, Plée D, Aubert T (2006) Mater Res Bull 41(3):478–484
155. Show Y, Imaizumi K (2007) Diam Relat Mater 16(4-7):1154–1158
156. Suematsu S, Machida K, Tamamitsu K (2008) JP PAT 5266844, 2013
157. Raymundo-Piñero E, Cadek M, Wachtler M, Béguin F (2011) ChemSusChem 4(7):943–949
158. Smithyman J, Moench A, Liang R, Zheng JP, Wang B, Zhang C (2012) Appl Phys A Mater Sci Process 107(3):723–731
159. Dolah BNM, Deraman M, Othman MAR, Farma R, Taer E, Awitdrus A, Basri NH, Talib IA, Omar R, Nor NSM (2014) Mater Res Bull 60:10–19
160. Quintero R, Kim DY, Hasegawa K, Yamada Y, Yamada A, Noda S (2014) RSC Adv 4(16):8230–8237
161. Quintero R, Kim DT, Hasegawa K, Yamada Y, Yamada A, Noda S (2015) RSC Adv 5(21):16101–16111
162. Lu W, Hartman R, Qu L, Dai L (2011) J Phys Chem Lett 2(6):655–660
163. Izadi-Najafabadi A, Yamada T, Futaba DN, Yudasaka M, Takagi H, Hatori H, Iijima S, Hata K (2011) ACS Nano 5(2):811–819
164. Shiraishi S, Kibe M, Yokoyama T, Kurihara H, Patel N, Oya A, Kaburagi Y, Hishiyama Y (2006) Appl Phys A Mater Sci Process 82(4):585–591
165. Gu WT, Sevilla M, Magasinski A, Fuertes AB, Yushin G (2013) Energy Environ Sci 6(8):2465–2476
166. Fan XM, Yu C, Ling Z, Yang J, Qiu JS (2013) ACS Appl Mater Interfaces 5(6):2104–2110
167. Hulicova D, Yamashita J, Soneda Y, Hatori H, Kodama M (2005) Chem Mater 17(5):1241–1247
168. Hulicova D, Kodama M, Hatori H, Shiraishi S (2009) Adv Funct Mater 19(11):1800–1809
169. Lee J, Yoon S, Hyeon T, Oh SM, Kim KB (1999) Chem Commun 21:2177–2178
170. Kodama M, Yamashita J, Soneda Y, Hatori H, Kamegawa K, Moriguchi I (2006) Chem Lett 35(6):680–681
171. Kodama M (2013) TANSO 258:171–178
172. Hulicova D, Kodama M, Hatori H (2006) Chem Mater 18(9):2318–2326
173. Soneda Y, Toyoda M, Hashiya K, Yamashita J, Kodama M, Hatori H, Inagaki M (2003) Carbon 41(13):2680–2682
174. Toyoda M, Tani Y, Soneda Y (2004) Carbon 42(14):2833–2837
175. Soneda Y, Yamashita J, Kodama M, Hatori H, Toyoda M, Inagaki M (2006) Appl Phys A Mater Sci Process 82(4):575–578
176. Toyoda M, Shimizu A, Iwata H, Inagaki M (2001) Carbon 39(11):1697–1707
177. Toyoda M, Katoh H, Inagaki M (2001) Carbon 39(14):2231–2234
178. Toyoda M, Sedlacik J, Inagaki M (2002) Synth Met 130(1):39–43
179. Huang Z-H, Zheng XY, Lv W, Wang M, Yang Q-H, Kang FY (2011) Langmuir 27(12):7558–7562
180. Jang BZ, Liu C, Neff D, Yu Z, Wang MC, Xiong W, Zhamu A (2011) Nano Lett 11(9):3785–3791
181. Yu JH, Xu LL, Zhu QQ, Wang XX, Yun MJ, Dong LF (2016) J Inorg Mat 31:220–224